

**Supplementary Information for**  
**Photosynthesis Assisted Remodeling of Three-Dimensional Printed Structures**

Kunhao Yu<sup>1†</sup>, Zhangzhengrong Feng<sup>1†</sup>, Haixu Du<sup>1</sup>, An Xin<sup>1</sup>, Kyung Hoon Lee<sup>1</sup>, Ketian Li<sup>1</sup>,  
Yipin Su<sup>1</sup>, Qiming Wang<sup>1\*</sup>, Nicholas X. Fang<sup>2\*</sup>, Chiara Daraio<sup>3\*</sup>

<sup>1</sup>Sonny Astani Department of Civil and Environmental Engineering, University of Southern California, Los Angeles, California 90089, United States.

<sup>2</sup>Department of Mechanical Engineering, Massachusetts Institute of Technology, Cambridge, Massachusetts 02139, United States.

<sup>3</sup>Division of Engineering and Applied Science, California Institute of Technology, Pasadena, California 91125, United States.

† Contribute equally.

\*Correspondence to: qimingw@usc.edu (Q. Wang); nicfang@mit.edu (N. X. Fang); daraio@caltech.edu (C. Daraio).

**This PDF file includes:**

- Materials and methods
- Supplementary analysis
- Figures S1 to S34
- Tables S1 to S2
- Captions for Movies S1 to S2
- References

**Other Supplementary Information for this manuscript include the following:**

- Movies S1 to S2

## Materials and Methods

**Materials.** Poly(tetrahydrofuran) (PolyTHF, average molar mass 650 g/mol), isophorone diisocyanate (IPDI), dimethylacetamide (DMAc), 2-Hydroxyethyl methacrylate (HEMA), dibutyltin dilaurate (DBTDL), 1,6-hexanediol diacrylate (HDDA),  $\alpha$ -D-Glucose, phenylbis(2,4,6-trimethylbenzoyl)phosphine oxide (photoinitiator), Sudan I (photoabsorber), HEPES buffer solution, Poly (ethylene glycol), Potassium phosphate tribasic ( $K_3PO_4$ ), Magnesium chloride ( $MgCl_2$ ), Sodium hydroxide (NaOH), Percoll (pH 8.5-9.5), and periodic acid ( $HIO_4$ ) were purchased from Sigma-Aldrich and used without further purification. Baby spinach leaves (*Spinacia oleracea* L.) were purchased from Trader Joe's.

**Extraction of chloroplasts.** The HEPES buffer solution was prepared by mixing HEPES buffer ( $30 \times 10^{-3}M$ , pH 5.0-6.0), poly(ethylene glycol) ( $M_w$ . 8000, 10% (w/v)),  $MgCl_2$  ( $2.5 \times 10^{-3} M$ ),  $K_3PO_4$  ( $0.5 \times 10^{-3} M$ ), and DI Water. The HEPES buffer solution was then magnetically stirred for 3 h. NaOH solution was added to adjust the pH value to be around 7.6. The HEPES buffer solution was then stored in the fridge at 4°C for 3 h before use. Then, the fresh baby spinach leaves (*Spinacia oleracea* L.) were washed with DI water and then dried to remove the surface water. Next, the middle veins of the leaves were removed to obtain 65 g leaf meat from about 100 g of fresh leaves. Then, the leaf meat was ground with 100 ml HEPES buffer solution in the pre-chilled kitchen blender for about 2 minutes until the mixture became homogeneous. The mixture was centrifuged with 4000 RPM for 15 min at 4 °C (Eppendorf 5804R). Then, the supernatant was removed, and the chloroplast pellet was re-suspended in the HEPES buffer solution. After adding the suspended mixture on the top of 5 mL of 40% Percoll in two pre-chilled tubes, we centrifuged the mixture at 3636 RPM for 8 min at 4 °C. Later, we removed the supernatant and kept the pellet. Next, we washed the pellet by adding 10 mL HEPES buffer solution and piped it out twice to remove Percoll. Before using the extracted chloroplast, we put the tubes upside down in the fridge for 1 h to get rid of the remained water or buffer solution from the chloroplast pellet.

**Preparation of polymer inks with and without free NCO groups.** To fabricate polymer inks with free NCO groups (**Fig. S1**), we preheated 0.01 mole of PolyTHF at 100°C and exposed to Nitrogen environment for 1 h to remove moisture and oxygen. 0.02 mole of IPDI, 10 wt% of DMAc and 1 wt% of DBTDL were mixed with the preheated PolyTHF at 70°C and stirred with a magnetic stir bar for 1 h. After reducing the temperature to 40°C, 0.01 mole of HEMA was added and mixed for 1 h to complete the synthesis. To fabricate polymer inks without free NCO groups (**Fig. S12**), we used a similar procedure as that of the polymer ink with free NCO groups except for 0.02 mole of HEMA in the last step. For the additive manufacturing, 2 wt% of photoinitiator (phenylbis(2,4,6-trimethylbenzoyl)phosphine oxide) was mixed with the polymer inks and stored in a dark amber glass bottle until use.

**Preparation of polymer inks with chloroplasts.** Extracted chloroplasts of various weight percent from 0 wt% to 7 wt% were gently mixed with the prepared polymer inks (with or without free NCO groups) using a magnetic stir bar for 30 min at 5°C in a dark environment to prevent the degradation of chloroplasts (**Fig. S2**).

**3D printing process.** A similar printing technique was described elsewhere (**Fig. S3**)<sup>12,13</sup>. A computer-aided design (CAD) model was designed and converted into an STL file, which was then sliced into an image sequence. The sliced images were then used to print the 3D

structure with a bottom-up stereolithography (SLA) printer. An image-patterned light with a wavelength of 405 nm was projected from the bottom to a resin bath that was filled with a synthesized polymer ink. A motor-controlled printing stage was mounted onto the resin bath with a prescribed liquid height. The light-exposed resin was solidified and bonded onto the printing stage. As the printing stage was lifted, the fresh resin refluxed beneath the printing stage. By lowering the printing stage at prescribed height and illuminating the resin with another slice image, a second layer was printed and bonded onto the first layer. These processes were repeated to form a 3D-architected structure. A Teflon membrane with low surface tension ( $\sim 20$  mN/m) was employed to reduce the separation force between the solidified part and the printing window.

**Photosynthesis process in different conditions.** The 3D-printed solid samples were placed in a white-light chamber (CL-1000 Ultraviolet Crosslinker with five UVP 34-0056-01 bulbs, light intensity  $69.3$   $W/m^2$ ) with different exposure conditions. For the experimental group and control 2 group in **Figs. 2A** and **2C**, the samples went through 4-h illumination of white light followed by 4-h darkness in the chamber. For the control 1 group in **Fig. 2B**, the samples went through 8-h darkness in the chamber. For the samples with chloroplasts of various weight concentrations (0-7 wt%, **Fig. 2I**), they went through 4-h light illumination and 4-h darkness. For the samples with various light-illumination periods (**Fig. 2J**), they went through periods of light illumination and darkness of the same length. For example, the 15-minutes group went through 15-minute light illumination and 15-minute darkness.

**Characterization of strengthening effect.** Dumbbell-like samples were fabricated with the aforementioned 3D-printing process (length 5 mm, width 2 mm, and thickness 2 mm shown in **Fig. S9A**). After the respective photosynthesis or non-photosynthesis processes described above, the samples were placed in a dark chamber ( $40^\circ\text{C}$ ) for 12 h to evaporate the residual solvent. Then, the samples were uniaxially stretched until rupture with a strain rate of  $0.05$   $s^{-1}$  using a mechanical tester (Instron, model 5942). Spectrum TWO FT-IR Spectrometer (PerkinElmer, USA) was used for the FT-IR analyses before and after the respective photosynthesis or non-photosynthesis processes with the scanning range of  $450$  to  $4000$   $cm^{-1}$  at a resolution of  $0.5$   $cm^{-1}$ .

The fracture energies of the polymers after different photosynthesis conditions were measured by using pure-shear fracture tests<sup>20,21</sup>. Unnotched and notched samples (length  $a_0 = 40$  mm, thickness  $b_0 = 1$  mm and distance between two clamps  $L_0 = 5$  mm) were employed (**Figs. S9B, S11**). The notched sample was prepared by using a razor blade to cut a 20-mm notch in the middle left region. Both samples were uniaxially stretched with a strain rate of  $0.05$   $s^{-1}$  until rupture. A camera was used to record the critical distance (denoted as  $L_c$ ) between the clamps when the crack starts propagating on the notched sample. The fracture energy was calculated as  $U(L_c)/(a_0 b_0)$ , where  $U(L_c)$  is the work done by the applied force before the critical distance, illustrated as the area beneath the force-distance curve in the unnotched test (**Fig. S11**).

**Verification of glucose production from the embedded chloroplasts.** The prepared polymer ink without free NCO groups (**Fig. S12**) was gently mixed with 5wt% of extracted chloroplasts with a magnetic stir bar for 30 min at  $5^\circ\text{C}$  in a dark environment to prevent the degradation of chloroplasts. The mixture was 3D-printed into dumbbell-like samples. The prepared samples were placed in a white-light chamber (light intensity  $69.3$   $W/m^2$ ) for two different conditions, including 4-h light illumination and 4-h darkness, and 8-h darkness. The

FTIR analyses were conducted to monitor the transmittance corresponding to the OH groups in the polymer samples at the as-fabricated state, after 4-h light and 4-h darkness, and after 8-h darkness (Figs. S13AB). After removing the residual solvent in a dark chamber (40°C) for 12 h, the samples were then uniaxially stretched until rupture with a strain rate of  $0.05 \text{ s}^{-1}$  (Fig. S13D).

**Characterization of polymer strengthened by glucose.**  $\alpha$ -D-glucose was first mixed with polymer ink with free NCO groups to make different glucose concentrations (0 M-0.389 M). The mixture was 3D-printed into dumbbell-like samples. The FTIR analyses were conducted to monitor the transmittance corresponding to the NCO groups in the polymer samples with different glucose concentrations. After removing the residual solvent in a dark chamber (40°C) for 12 h, the samples were then uniaxially stretched until rupture with a strain rate of  $0.05 \text{ s}^{-1}$ .

**Effects of chloroplast concentration and illumination time.** The fabricated polymer samples with free NCO groups and chloroplasts of various weight concentrations (0-7wt%) were uniaxially stretched until rupture with a strain rate of  $0.05 \text{ s}^{-1}$  after 4-h light illumination and 4-h darkness. The fabricated polymer samples with free NCO groups and 5 wt% chloroplasts after undergoing various light illumination periods (0-6 h) and the respective darkness periods (same length of the illumination period), were also uniaxially stretched until rupture with a strain rate of  $0.05 \text{ s}^{-1}$ . The Young's modulus and tensile strength of each sample were calculated from the obtained tensile stress-strain curve.

**Freezing chloroplasts with a chilling temperature.** The fabricated polymer samples with free NCO groups and 5 wt% chloroplasts were first sealed in a petri dish and then immersed in an ice bath. The samples with the temperature of 0-4°C underwent 2-h light illumination and 2-h darkness. These samples were divided into two parts. Some processed samples were uniaxially stretched until rupture with a strain rate of  $0.05 \text{ s}^{-1}$ . For other processed samples, the temperature was first raised to room temperature (25°C); and then these samples underwent another 2-h light illumination and 2-h darkness, followed by being uniaxially stretched until rupture with a strain rate of  $0.05 \text{ s}^{-1}$ .

**Cleavage of glucose crosslinkers in the strengthened polymer.** The strengthened polymer samples were immersed in a 2 M periodic acid solution (2 moles of periodic acid and 1 L of DMAc) for 6 h. The samples were swollen by around 220% and then de-swollen by evaporating the residual solvent in a dark chamber (40°C) for 12 h. For the control group, the strengthened samples were immersed in the DMAc solvent for 6 h and then de-swollen by evaporating the solvent in a dark chamber (40°C) for 12 h. Both sets of samples were then uniaxially stretched until rupture with a strain rate of  $0.05 \text{ s}^{-1}$ .

**Local strengthening with an "S" shape.** Plate samples (with free NCO groups and 5 wt% embedded chloroplasts) with a size of 14mm  $\times$  10mm  $\times$  2mm were fabricated by the aforementioned 3D-printing system (Fig. 3B). The samples were then placed in an amber container, covered with a mask with an "S" shape, and put in the white-light chamber for 4-h illumination and 4-h darkness. Young's modulus distribution over the sample surface was measured by using a round-flat end cylinder indenter with radius  $R=0.5 \text{ mm}$  loaded on the Instron mechanical tester to indent the sample by applying force  $F$  to certain indentation depth  $\delta$ . The Young's modulus of each location was calculated as  $E = F(1 - \nu^2)/(2R\delta)$ , where  $\nu =$

0.48 is the Poisson's ratio of material (SI appendix, Fig. S26). The Young's modulus distribution map was plot using MATLAB (Fig. 3C).

**Local strengthening with circles.** Plate samples (with free NCO groups and 5 wt% embedded chloroplasts) with sizes of 20 mm × 20 mm × 2 mm (for Fig. 3E) and 56 mm × 20 mm × 2 mm (for Fig. 3H) were fabricated by the aforementioned 3D-printing system. The 20 mm × 20 mm × 2 mm sample was locally strengthened with a circular-shaped mask (circle diameter = 3 mm) next to a 3-mm edge notch. The 56 mm × 20 mm × 2 mm sample was locally strengthened with 18 circular patterns (circle diameter = 1 mm) with a certain path next to an edge notch. Both samples were then clamped at the left two corners for the tearing test with the Instron mechanical tester.

**Homogeneous and graded lattice structures.** Lattice structures (with free NCO groups and 5 wt% embedded chloroplasts) with various units (2 × 2 × 1 for Fig. S27 and 10 × 4 × 1 for Fig. 3J) were fabricated by the aforementioned 3D-printing system. For the structures with homogeneous light, the printed samples were placed in the white-light chamber with 2-h illumination on the front side and 2-h illumination on the rear side, followed with 4 h darkness. For the structure with the darkness condition, the printed samples were placed in the dark chamber for 8 h. For the structures treated with a graded light, a transparent cover was attached with different layers of vinyl-coated white tape and covered on top of the printed sample (Fig. S28). The entire setup was then placed in the white-light chamber to induce a graded light intensity varies from 0 to 69.3 W/m<sup>2</sup> on the long edge direction of the sample for each unit distance (2 mm). The samples were placed in the graded light chamber with 2-h illumination on the front side and 2-h illumination on the rear side, followed with 4 h darkness.

The 2 × 2 × 1 lattice structures with different conditions were tested under a compressive load along the longitudinal direction (gradient direction) with a strain rate of 0.05 s<sup>-1</sup> using the Instron mechanical tester (Fig. S27). The Young's modulus of each unit of the 10 × 4 × 1 lattice structures was tested lattice by the indentation test. The Young's modulus can be calculated as  $E = F(1 - \nu^2)/(2R\delta)$ , where  $F$  is the applied load,  $\nu = 0.48$  is the effective Poisson's ratio,  $R$  is the radius of a round-flat end cylinder indenter ( $R=1$  mm), and  $\delta$  is the indentation depth.

The energy absorption behaviors of the 10 × 4 × 1 lattices were characterized by impact loading tests with a relatively large strain rate of 10 mm/s. The absorbed energy was calculated by the area underneath the load-displacement curves (Fig. 3L).

**3D-printing and strengthening of tree-like structures.** The tree-like structures were fabricated by the aforementioned 3D printing system using the polymer ink with free NCO groups and 5 wt% embedded chloroplast. The printed tree-like structures were then placed in a white-light chamber with 2-h light illumination (light intensity 69.3 W/m<sup>2</sup>) and 2-h darkness. To characterize the load sustaining capability of the tree-like structures in different states, we hang a 1-g metal ring on one tree branch at the unstrengthened state (with 4-h darkness) and after photosynthesis process (2-h illumination and 2-h darkness).

**3D-printing and strengthening of Popeye-like structures.** The Popeye-like structures (height 23 mm, width 15 mm, and depth 5 mm) were fabricated by the aforementioned 3D printing system using the polymer ink with free NCO groups and 5 wt% embedded chloroplast. The printed Popeye-like structures were then placed in a white-light chamber with 2-h light illumination (light intensity 69.3 W/m<sup>2</sup>) and 2-h darkness. To characterize the weight sustaining

capability of the Popeye-like structures in different states, we loaded a 200-g weight (two weights of 100 g each) on a glass slide that was placed on the strengthened or unstrengthened Popeye-like structures.

**Effect of pre-stretch on Photosynthesis-assisted strengthening.** The fabricated polymer samples with free NCO groups and 5 wt% chloroplasts were first uniaxially pre-stretched with various stretches ( $\lambda = 1 - 1.3$ ) and undergone 4-h light illumination and 4-h darkness. Then, the processed samples were then cut into smaller samples with a dumbbell-like shape, which were uniaxially stretched until rupture with a strain rate of  $0.05 \text{ s}^{-1}$ . The FTIR analyses were conducted to monitor the transmittance corresponding to the NCO groups in the polymer samples with different pre-stretches.

**Photosynthesis-assisted strengthening under a non-uniform pre-stress distribution.** Plate sample (with free NCO groups and 5 wt% embedded chloroplasts) with a size of  $12 \text{ mm} \times 8 \text{ mm} \times 2 \text{ mm}$  was fabricated by the aforementioned 3D-printing system. A foot-like 3D structure with non-uniform surface was also 3D-printed with a rigid polymer ink (HDDA). The foot-like structure was compressed on the sample plate by deforming 1 mm in depth. The deformation-induced a non-uniform stress-distribution on the sample plate. With the deformation, the plate illuminated by white light (light intensity  $69.3 \text{ W/m}^2$ ) from the bottom for 4 h, followed by 4-h darkness. Young's modulus distribution over the sample surface was measured by using a round-flat end cylinder indenter with radius  $R=0.5 \text{ mm}$  loaded on the Instron mechanical tester (**Fig. S26**).

**Characterization of Photosynthesis-assisted healing.** 3D printed dumbbell-shaped samples with free NCO groups and 5wt% embedded chloroplasts were first cut into two parts with a razor blade, and the fractured surfaces were brought into contact immediately. The samples were then placed in a white-light chamber with light illuminating time various from 1 h to 8 h, followed by the darkness with the same respective period. For the control, 3D printed dumbbell-shaped samples with free NCO groups but without embedded chloroplasts were used. Both healed and control samples were uniaxially stretched to rupture with the same strain rate ( $0.05 \text{ s}^{-1}$ ). An optical microscope (Nikon Eclipse LV100ND) was used to image the healing region (**Fig. 5B**).

**Photosynthesis-assisted healing of 3D-printed propeller.** The 3D-printed propellers were fabricated by the aforementioned 3D printing system. The experiment propellers were fabricated using polymer inks with free NCO groups and 5wt% embedded chloroplasts. 4-mm damages were introduced on each sector of the printed propellers with a razor blade. The fractured surfaces were aligned into contact immediately and then placed in a white-light chamber with 4-h light illumination and 4-h darkness. Two healed propellers were assembled onto a remotely controlled boat to provide the pushing force to move forward in a pound (**Fig. 5F**). The control propellers were fabricated using polymer inks with free NCO groups but without chloroplasts. The controlled propellers were also damaged, healed, and assembled onto the remotely controlled boat (**Fig. 5G**).

## Supplementary analysis

### Mathematical model of polymer strengthening by additional crosslinking

In the current work, the polymer ink is first crosslinked by the photo-initiated addition reaction of the acrylate groups (**Fig. S2**). Within this primary polymer network, NCO groups are active sites that can have a strong reaction with hydroxyl groups (OH) on the chloroplast-produced glucose to form urethane linkages (-NH-CO-O-). Since a glucose molecule has multiple OH groups, it is hypothesized that the OH groups on the chloroplast-produced glucose can bridge multiple NCO groups to create new crosslinks additional to the acrylate-enabled crosslinks within the designed polymer matrix (**Fig. S17A**).

#### (1) Before strengthening

Before strengthening, the polymer network is assumed to feature a homogenous chain length. The chain length is described by the Kuhn length, denoted as  $N_0$  and chain number per unit volume as  $n_0$ . The strain energy density of the polymer network can be written as <sup>1,2</sup>

$$W_0 = n_0 k_B T N_0 \left( \frac{\beta_0}{\tanh \beta_0} + \ln \frac{\beta_0}{\sinh \beta_0} \right) \quad (\text{S1})$$

where  $k_B$  is the Boltzmann constant,  $T$  is the temperature in Kelvin, and

$$\beta_0 = L^{-1} \left( \frac{\Lambda}{\sqrt{N_0}} \right) \quad (\text{S2})$$

where  $L^{-1}(\ )$  is the inverse Langevin function and  $\Lambda$  is the chain stretch. Here, we follow an affine deformation assumption that the microscopic polymer chain deformation affinely follows the macroscopic deformation in three principal directions; thus, the chain stretch can be expressed as

$$\Lambda = \sqrt{\lambda_1^2 + \lambda_2^2 + \lambda_3^2} \quad (\text{S3})$$

This affine deformation assumption has been widely adopted for deriving the constitutive models for rubber-like materials, such as the New-Hookean model <sup>1</sup> and the Arruda-Boyce model <sup>2</sup>. The chain stretch expressed in Eq. S3 is directly adopted from the New-Hookean model <sup>1,3</sup>.

If the polymer is incompressible, the Cauchy stresses in three principal directions can be written as

$$\begin{cases} \sigma_1 = \lambda_1 \frac{\partial W_0}{\partial \lambda_1} - P \\ \sigma_2 = \lambda_2 \frac{\partial W_0}{\partial \lambda_2} - P \\ \sigma_3 = \lambda_3 \frac{\partial W_0}{\partial \lambda_3} - P \end{cases} \quad (\text{S4})$$

where  $P$  is the hydrostatic pressure. Under uniaxial tension with  $\lambda_1 = \lambda$  and  $\lambda_2 = \lambda_3 = \lambda^{-1/2}$ , the Cauchy stresses  $\sigma_2$  and  $\sigma_3$  vanish. The Cauchy stress  $\sigma_1$  can be formulated as

$$\sigma_1 = \lambda_1 \frac{\partial W_0}{\partial \lambda_1} - \lambda_2 \frac{\partial W_0}{\partial \lambda_2} \quad (\text{S5})$$

The corresponding tensile nominal stress (engineering stress) can be calculated as

$$s_1 = \frac{\sigma_1}{\lambda_1} = n_0 k_B T \sqrt{N_0} \frac{\lambda - \lambda^{-2}}{\sqrt{\lambda^2 + 2\lambda^{-1}}} L^{-1} \left( \sqrt{\frac{\lambda^2 + 2\lambda^{-1}}{N_0}} \right) \quad (\text{S6})$$

Equation S6 can be used to explain the stress-strain behaviors of polymer samples before strengthening. Only two fitting parameters (polymer chain length  $N_0$  and chain number density  $n_0$ ) are required.

## (2) Strengthening by forming additional crosslinks

Once the glucose is introduced, additional crosslinks form through the reactions between the free NCO groups and the OH groups on the glucose (**Fig. S17A**). One glucose molecule with 5 OH groups is only required to bridge two NCO groups to form a crosslink. Thus, one glucose molecule is able to at most form 2.5 crosslinks within the network. The number of the introduced glucose molecules per unit volume is denoted as  $n_g$  and the formed additional crosslink number per unit volume is denoted as  $n_a$ , which should follow  $n_g \leq n_a \leq 2.5n_g$ .

As shown in **Fig. S17B**, two polymer chains with chain length  $N_0$  become four polymer chains with shorter lengths after introducing an additional crosslink. In a general case, these four polymer chains may have different chain lengths. Here, to capture the essential physics with a simple mathematic formulation, we assume these four polymer chains have the same chain length, as  $N_0/2$ . In a more general case shown in **Fig. S17C**, we assume the crosslink formed between a chain with a length of  $N_0/2^i$  and a chain with a length of  $N_0/2^j$  induces four chains with respective half lengths, where  $i = 0, 1, 2 \dots$  and  $j = 0, 1, 2 \dots$ .

After introducing  $n_a$  additional crosslinks per unit volume, the initially homogeneous chain length ( $N_0$ ) will become inhomogeneous, with a chain length distribution over lengths of  $N_0$ ,  $N_0/2$ ,  $\dots$ , and  $N_0/2^m$ , where  $m \geq 1$ . The value of  $m$  is constrained by choosing the largest  $m$  to ensure

$$\frac{N_0}{2^m} \geq N_{min} \quad (\text{S7})$$

where  $N_{min}$  is the admissible smallest chain length.

To estimate the chain number of each type of chain length per unit volume, we treat the additional crosslinking process as  $m$  steps. In each step, additional crosslinks of a certain amount are introduced. We employ two methods:

### Method 1: Equal number of incremental crosslinks

In method 1, we assume that probabilities of forming a crosslink on the chain with a length of  $N_0/2^i$  and the chain with a length of  $N_0/2^j$  are equal, where  $i = 0, 1, 2 \dots$  and  $j = 0, 1, 2 \dots$ . Under this assumption, the incremental additional crosslinking density for each step is equal, denoted as  $dn_a$ :

$$dn_a = \frac{n_a}{m} \quad (\text{S8})$$

In the following, we will go through each step to calculate the volume density of polymer chains with length  $N_0/2^j$ , where  $j = 0, 1, 2 \dots$ . We denote it as  $C_j$ , where  $j = 0, 1, 2 \dots$ .



In step 1, some of the initial chains with length  $N_0$  become shorter chains with a length of  $N_0/2$  after adding  $dn_a$  crosslinks if  $2dn_a \leq n_0$ . At the end of step 1, we have:

$$C_0 = n_0 - 2dn_a \quad (\text{S9a})$$

$$C_1 = 4dn_a \quad (\text{S9b})$$

In step 2, three possible routes to form crosslinks: between two chains with the length of  $N_0$ , between two chains with the length of  $N_0/2$ , and between a chain with the length of  $N_0$  and a chain with the length of  $N_0/2$ . The probabilities for partitioning chains with length  $N_0$  and chains with length  $N_0/2$  are equal. Therefore, at the end of step 2, we have:

$$C_0 = n_0 - 2dn_a - 2(dn_a/2) \quad (\text{S10a})$$

$$C_1 = 4dn_a + 4(dn_a/2) - 2(dn_a/2) \quad (\text{S10b})$$

$$C_2 = 4(dn_a/2) \quad (\text{S10c})$$

Similarly, at the end of step 3, we have:

$$C_0 = n_0 - 2dn_a - 2(dn_a/2) - 2(dn_a/3) \quad (\text{S11a})$$

$$C_1 = 4dn_a + 4(dn_a/2) - 2(dn_a/2) + 4(dn_a/3) - 2(dn_a/3) \quad (\text{S11b})$$

$$C_2 = 4(dn_a/2) + 4(dn_a/3) - 2(dn_a/3) \quad (\text{S11c})$$

$$C_3 = 4(dn_a/3) \quad (\text{S11d})$$

Eventually, at the end of step  $m$ , we have:

$$C_0 = n_0 - 2dn_a \left(1 + \frac{1}{2} + \frac{1}{3} + \dots + \frac{1}{m}\right) \quad (\text{S12a})$$

$$C_1 = 2dn_a + 2dn_a \left(1 + \frac{1}{2} + \frac{1}{3} + \dots + \frac{1}{m}\right) \quad (\text{S12b})$$

$$C_2 = 2\left(\frac{dn_a}{2}\right) + 2dn_a \left(\frac{1}{2} + \frac{1}{3} + \dots + \frac{1}{m}\right) \quad (\text{S12c})$$

.....

$$C_j = 2(dn_a/j) + 2dn_a \left(\frac{1}{j} + \frac{1}{j+1} + \dots + \frac{1}{m}\right) \quad (\text{S12d})$$

.....

$$C_m = 4(dn_a/m) \quad (\text{S12e})$$

The volume density of chains with length  $N_0/2^j$  at the end of step  $m$  can be summarized as

$$C_j = \begin{cases} n_0 - \frac{2n_a}{m} \left(1 + \frac{1}{2} + \frac{1}{3} + \dots + \frac{1}{m}\right), j = 0 \\ \frac{2n_a}{m} \left(\frac{2}{j} + \frac{1}{j+1} + \dots + \frac{1}{m}\right), 1 \leq j \leq m-1 \\ \frac{4n_a}{m^2}, j = m \end{cases} \quad (\text{S13})$$

After strengthening, the polymer chain length is inhomogeneous with a chain length distribution over lengths of  $N_0$ ,  $N_0/2$ , ..., and  $N_0/2^m$ , where  $m \geq 1$ . The chain length distribution is shown in Eq. S13. We assume that under deformation, each polymer chain deform following an affine deformation assumption that the microscopic polymer chain deformation affinely follows the macroscopic deformation in three principal directions; thus, the chain stretch of the chain with the length of  $N_0/2^j$  ( $j = 0, 1, 2 \dots$ ) can be expressed as<sup>4-10</sup>

$$\Lambda_j = \sqrt{\lambda_1^2 + \lambda_2^2 + \lambda_3^2} \quad (\text{S14})$$

The strain energy of the whole polymer network per unit volume can be formulated as<sup>4-10</sup>

$$W_s = \sum_{j=0}^m \left[ C_j k_B T \left( \frac{N_0}{2^j} \right) \left( \frac{\beta_j}{\tanh \beta_j} + \ln \frac{\beta_j}{\sinh \beta_j} \right) \right] \quad (\text{S15})$$

$$\beta_j = L^{-1} \left( \frac{\Lambda_j}{\sqrt{N_0/2^j}} \right) \quad (\text{S16})$$

where the chain stretch  $\Lambda_j$  is given in Eq. S14. Under uniaxial tension with  $\lambda_1 = \lambda$  and  $\lambda_2 = \lambda_3 = \lambda^{-1/2}$ , the nominal tensile stress of the incompressible polymer after strengthening can be calculated as

$$s_{s1} = \sum_{j=0}^m \left[ C_j k_B T \sqrt{N_0/2^j} \frac{\lambda - \lambda^{-2}}{\sqrt{\lambda^2 + 2\lambda^{-1}}} L^{-1} \left( \sqrt{\frac{\lambda^2 + 2\lambda^{-1}}{N_0/2^j}} \right) \right] \quad (\text{S17})$$

In method 1, there is a requirement for the relationship between  $n_a$  and  $m$ . For example, if  $m = 1$ , the maximal possible crosslinking point density is  $n_0/2$ . This condition is to ensure the chain density of chains with length  $N_0$  is not negative. For a certain  $m \geq 1$ , the requirement of the possible crosslink density is

$$(m - 1) / \left[ 2 \left( 1 + \frac{1}{2} + \frac{1}{3} + \dots + \frac{1}{m-1} \right) \right] < n_a/n_0 \leq m / \left[ 2 \left( 1 + \frac{1}{2} + \frac{1}{3} + \dots + \frac{1}{m} \right) \right] \quad (\text{S18})$$

## Method 2: Unequal number of incremental crosslinks

In method 2, we assume that the probability of forming a crosslink on the chain with the length of  $N_0/2^i$  is higher than that of forming a crosslink on the chain with the length of  $N_0/2^j$  when  $i < j$ . In an extreme case, the crosslink occurs first on the chain with the length of  $N_0/2^i$ , and then on the chain with the length of  $N_0/2^{i+1}$ . In other words, the crosslinking reaction on the longer chains always happens before the crosslinking reaction on the shorter chains. Following the assumption, we can naturally define the  $i$ th step as the step with the occurrence of the crosslinking reaction on the chain with the length of  $N_0/2^{i-1}$ . The process will move to the next step only when there are enough crosslinkers to consume all the chains with the length of  $N_0/2^{i-1}$ .

If the crosslinking reaction stops at step 1, there are only two types of chains: chains with length  $N_0$  and  $N_0/2$ . Their volume densities can be calculated as

$$C_0 = n_0 - 2n_a \quad (\text{S19a})$$

$$C_1 = 4n_a \quad (\text{S19b})$$

The requirement is  $0 < n_a/n_0 \leq 1/2$ .

If the crosslinking reaction stops at step 2, there are only two types of chains: chains with length  $N_0/2$  and  $N_0/2^2$ . Their volume densities can be calculated as

$$C_1 = 2n_0 - 2\left(n_a - \frac{n_0}{2}\right) = 3n_0 - 2n_a \quad (\text{S20a})$$

$$C_2 = 4\left(n_a - \frac{n_0}{2}\right) \quad (\text{S20b})$$

The requirement is  $1/2 < n_a/n_0 \leq 3/2$ .

If the crosslinking reaction stops at step  $m$ , at the end of step  $m$ , there are only two types of chains: chains with lengths  $N_0/2^{m-1}$  and  $N_0/2^m$ . Their volume densities can be calculated as

$$C_{m-1} = 2^{m-1}n_0 - 2\left[n_a - \left(2^{m-2} - \frac{1}{2}\right)n_0\right] = (2^m - 1)n_0 - 2n_a \quad (\text{S21a})$$

$$C_m = 4\left[n_a - \left(2^{m-2} - \frac{1}{2}\right)n_0\right] = 4n_a - 4\left(2^{m-2} - \frac{1}{2}\right)n_0 \quad (\text{S21b})$$

The requirement is for the additional crosslink density to reach step  $m$  is

$$\frac{2^{m-1}-1}{2} < n_a/n_0 \leq \frac{2^m-1}{2} \quad (\text{S22})$$

After strengthening, the strain energy function can be formulated as <sup>4-10</sup>

$$W_s = \sum_{j=m-1}^m \left[ C_j k_B T \left( \frac{N_0}{2^j} \right) \left( \frac{\beta_j}{\tanh \beta_j} + \ln \frac{\beta_j}{\sinh \beta_j} \right) \right] \quad (\text{S23})$$

$$\beta_j = L^{-1} \left( \frac{\Lambda_j}{\sqrt{N_0/2^j}} \right) \quad (\text{S24})$$

where the chain stretch  $\Lambda_j$  is given in Eq. S14 and  $C_j$  for  $j = m - 1$  and  $j = m$  are given in Eq. S21. Under uniaxial tension with  $\lambda_1 = \lambda$  and  $\lambda_2 = \lambda_3 = \lambda^{-1/2}$ , the nominal tensile stress of the incompressible polymer after strengthening can be calculated as

$$s_{s1} = \sum_{j=m-1}^m \left[ C_j k_B T \sqrt{N_0/2^j} \frac{\lambda - \lambda^{-2}}{\sqrt{\lambda^2 + 2\lambda^{-1}}} L^{-1} \left( \sqrt{\frac{\lambda^2 + 2\lambda^{-1}}{N_0/2^j}} \right) \right] \quad (\text{S25})$$

### (3) Theoretical results

#### Strengthening with $m=1$

When  $n_a/n_0 \leq 1/2$ , there is only one-step strengthening. After the strengthening, only chains with lengths of  $N_0$  and  $N_0/2$  coexist in the system. The strengthening can be modeled by either method 1 or method 2. As shown in **Figs. S18AB**, the polymer with an initial chain length  $N_0 = 100$  becomes stronger after forming more additional crosslinks. The Young's modulus (within 10% strain region) increases linearly with increasing the crosslink density (**Fig. S18B**).

We define the strengthening factor as the strengthened Young's modulus normalized by the unstrengthened Young's modulus. We find that the strengthening factor decreases with increasing the initial chain length  $N_0$  (**Figs. S18CD**). When the initial chain length  $N_0$  is very small, the polymer can be significantly strengthened. According to the stress-strain curve shapes of the studied polymers in this work (**Figs. S16**), the initial chain length should be  $N_0 \geq 60$ . The initial chain length cannot be too small. When the initial chain length  $N_0 > 500$ , the strengthening factor reaches a plateau of around 1.96. When the initial chain length  $60 \leq N_0 \leq 2000$ , the strengthening factor varies from 1.96 to 2.2.

According to the results shown in **Figs. 2G-J and S16**, the strengthening factor of the studied polymer in this work can reach as high as 6.2; therefore, we have to study the cases for  $m > 1$ .

### Strengthening with $m > 1$

When the density of the formed additional crosslinks  $n_a/n_0 > 1/2$ , the chain length distributions modeled by methods 1 and 2 are different. **Figure S19** shows the relationships between step number  $m$  and the density of the formed additional crosslinks for methods 1 and 2. For method 1, when  $n_a/n_0$  increases to 5, the step number  $m$  drastically increases to 45. However, the step number  $m$  is still 4 when  $n_a/n_0 = 5$  for method 2.

When  $n_a/n_0$  is slightly larger than  $1/2$  (e.g.,  $2/3$ ), the strengthening factors calculated from methods 1 and 2 are still almost the same (**Fig. S20**). However, when  $n_a/n_0$  increases to 1, the strengthening factors calculated from methods 1 are larger than those calculated from method 2 (**Figs. S21A-D**). It is because that the step number of method 1 is larger, corresponding to shorter chains.

When  $n_a/n_0$  is relatively large (e.g., 3.05), the step number for method 1 is 21, which means that the shortest chain length becomes  $N_0/2^{21}$ . Considering the stress-strain curve shape of studied polymer (**Figs. S16**), the initial chain length  $N_0$  is estimated between 60 and 2000.  $N_0/2^{21}$  becomes an invalid number for the chain length. Therefore, under such a situation that additional crosslink density is relatively large, method 1 cannot model the strengthening behavior. We can only employ method 2 (**Figs. S21EF**).

### (4) Comparison between theory and experiment

Using method 2, we can explain the stress-strain curves and Young's moduli of the polymers before and after strengthening (used parameters shown in **Table S2**). For example, for polymers with chloroplasts of various weight concentrations (0 to 5 wt%), the theoretically calculated stress-strain curves and Young's moduli agree with the respective experimental results (**Fig. S22AB**). It also works for polymers with 5 wt% chloroplasts under various illumination periods from 0 to 2 h (**Fig. S22CD**).

### Supplies of water and carbon dioxide

Since the chloroplasts are embedded in the polyurethane-based polymer matrix, external water supply cannot be provided to support the photosynthesis of the chloroplasts. The water for the photosynthesis process should be supplied by the water storage within the chloroplasts<sup>11-14</sup>. To estimate the mass percentage of water within the extracted chloroplast, we placed the extracted chloroplast in a dark environment and applied a gentle airflow to evaporate the water for 8 h. Through measuring the mass before and after the evaporation process, we estimated the mass percentage of the water within the extracted chloroplast was  $83.9 \pm 2.5$  wt% (**Table S1**). If the weight percentage of the chloroplast is 5 wt%, with the density of polyurethane-based polymer as  $1.25 \text{ g/cm}^3$ , we can roughly estimate the volume density of water supply as

$$C_{H_2O}^0 = \frac{5\% \times 83.9\% \times 1.25 \text{ g/cm}^3}{18 \text{ g/mol}} = 2.91 \text{ mol/L} \quad (\text{S26})$$

In plants, the carbon dioxide is digested by stomas and then gradually diffuse into cells at a deeper location<sup>12-14</sup>. In this study, since the polyurethane-based polymer has a relatively high permeability for carbon dioxide, with the diffusivity experimentally measured as  $D = 3.5 \times 10^{-7} - 3.9 \times 10^{-7} \text{ cm}^2 \text{ s}^{-1}$ <sup>15,16</sup>, we hypothesize that the carbon dioxide that supports photosynthesis may be provided by the existing carbon dioxide within the polymer matrix and the diffusion of carbon dioxide through the polymer matrix during the photosynthesis process. The concentration of carbon dioxide in the atmosphere in year 2019 was around 410-415 ppm<sup>17</sup>, which calculated as

$$C_{CO_2}^0 = 9.318 \times 10^{-3} - 9.432 \times 10^{-3} \text{ mol/L} \quad (\text{S27})$$

At the as-fabricated state, we assume the carbon dioxide within the polymer matrix is already in equilibrium with that in the atmosphere. During the photosynthesis process, the carbon dioxide within the polymer matrix is gradually consumed, and external carbon dioxide diffuses from the atmosphere into the polymer matrix.

The key question is whether the supplies of water and carbon dioxide are sufficient for the conducted experiment. To answer this question, we carry out the following estimation.

According to the theoretical modeling shown in above section, the initial chain density is estimated as  $n_0 = 4.5 \times 10^{19} \text{ m}^{-3} = 7.475 \times 10^{-8} \text{ mol/L}$  (**Table S2**). The concentration of the required additional crosslinks  $n_a$  for strengthening the polymer network with 5 wt% embedded chloroplasts should scale with  $n_0$ , written as

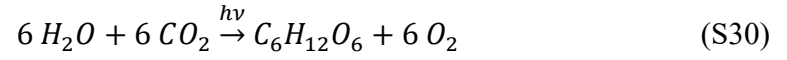
$$n_a = \beta n_0 \quad (\text{S28})$$

where  $\beta$  is a parameter ( $<10$ ) dependent on the light illumination time. For example, for 2-h light illumination,  $\beta = 2.3$ ; and for 4-h light illumination,  $\beta = 3 - 3.5$ .

One glucose molecule with 5 OH groups is only required to bridge two NCO groups to form a crosslink. Thus, one glucose molecule is able to at most form 2.5 crosslinks within the network. The number of the introduced glucose molecules per unit volume is denoted as  $n_g$ , which follows  $n_g \leq n_a \leq 2.5n_g$ . Therefore, the possible highest concentration of the required glucose is

$$n_g = n_a = \beta n_0 \quad (\text{S29})$$

For a photosynthesis process, the overall effective chemical reaction can be written as <sup>12-14</sup>



Equation S30 shows that the production of 1 glucose molecule requires 6 water molecules and 6 carbon dioxide molecules. Therefore, the concentrations of the required water and carbon dioxide are estimated as

$$C_{H_2O}^r = C_{CO_2}^r = 6\beta n_0 \quad (S31)$$

For 4-h light illumination (along with the subsequent 4-h darkness),  $6\beta n_0 \sim 1.35 \times 10^{-6} - 1.57 \times 10^{-6} \text{ mol/L}$ . Then, we have

$$C_{H_2O}^r \ll C_{H_2O}^0 \quad (S32)$$

$$C_{CO_2}^r < C_{CO_2}^0 \quad (S33)$$

Therefore, the supplies of water and carbon dioxide are sufficient for the experiment with 4-h light illumination (and 4-h darkness) in this work.

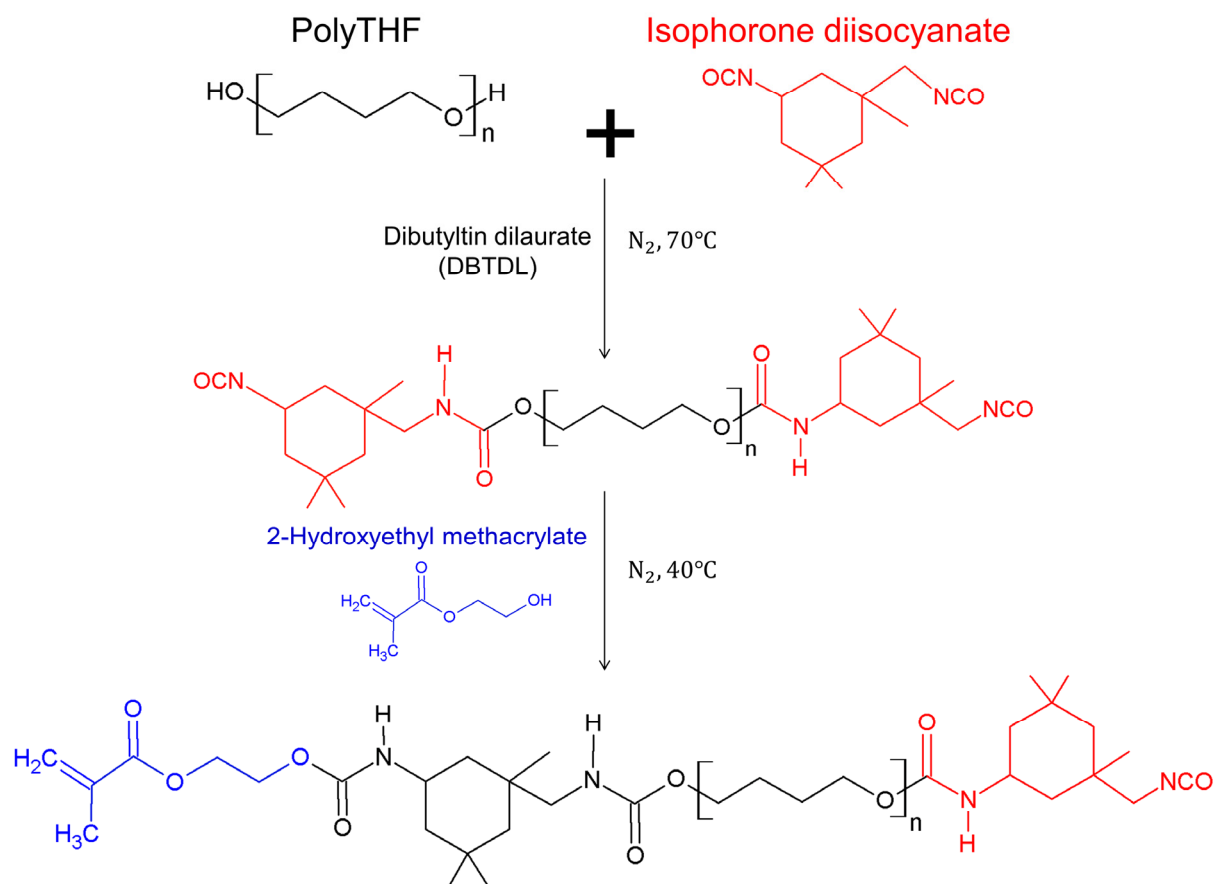


**Figure S1. Synthesis of polymer resin with acrylate and isocyanate (NCO) groups.** 0.01 mole of PolyTHF was preheated at 100°C and exposed to a nitrogen environment for 1 h to remove moisture and oxygen. 0.02 mole of IPDI, 10 wt% of DMAc and 1 wt% of DBTDL were mixed with preheated PolyTHF at 70°C and stirred with a magnetic stir bar for 1 h. After reducing the temperature to 40°C, 0.01 mole of HEMA was added and mixed for 1 h to complete the synthesis.

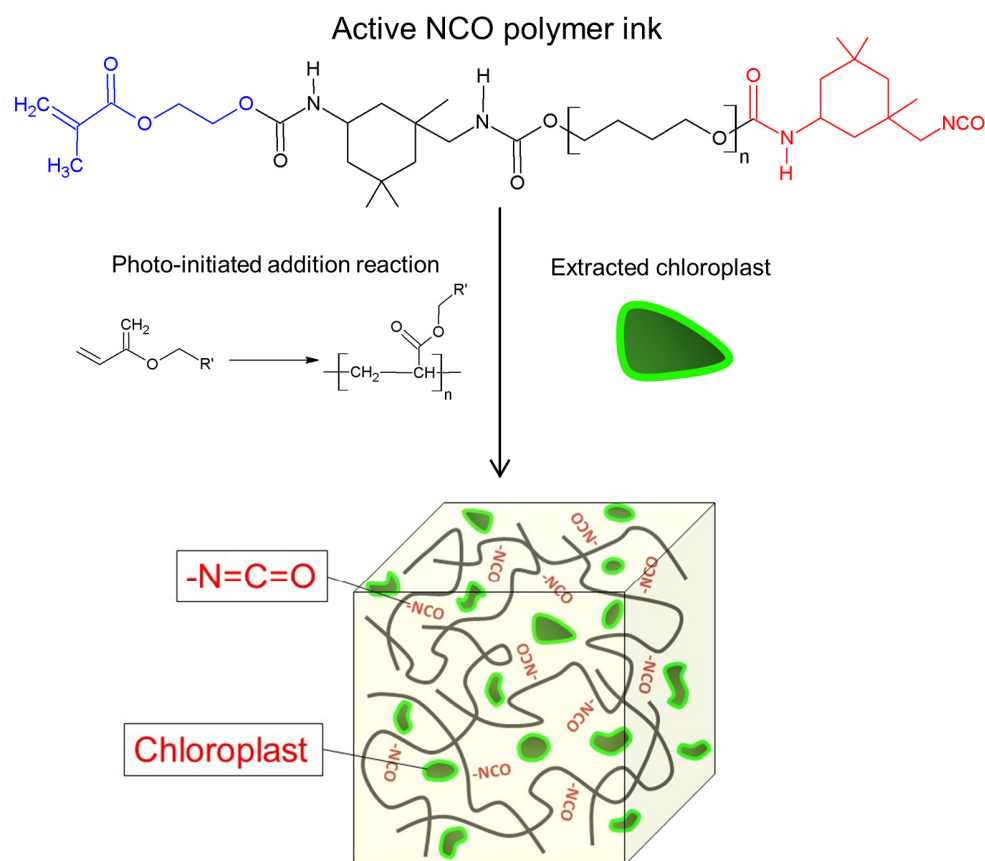


**Figure S2. Preparation of experiment polymer sample.** Extracted spinach chloroplasts were gently mixed with prepared polymer resin with acrylate and NCO groups by using a magnetic stir bar for 30 min at 5°C in a dark environment to prevent the degradation of chloroplasts. The mixed polymer resin then went through a photoradical-initiated addition reaction with the photopolymerization-based stereolithography system to photopolymerize the polymer resin.



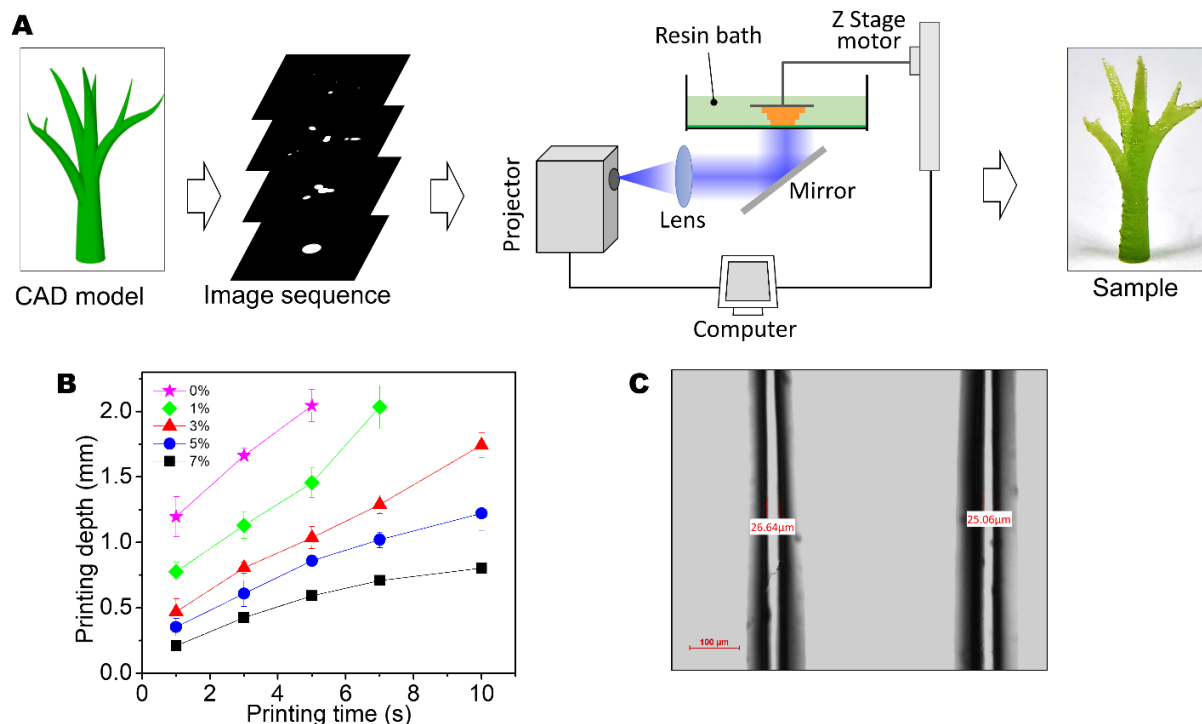


**Figure S3. (A)** 3D-printing of polymer structures. A CAD model was first sliced into a sequence of images. These 2D slice images, illuminated with UV/blue light from a light-emitting diode, were sequentially projected onto a transparent window. On the window, the liquid photoresin, capped into a prescribed height by a printing stage, was cured by the light and attached to the printing stage. As the printing stage was lifted off, the fresh resin refluxed beneath the printing stage. By lowering down the stage by a prescribed height and illuminating the resin with a subsequent slice image, a new layer could be printed and bonded onto the former layer. To eliminate the adhesion between the solidified resin and bath, we attached an oxygen-permeable membrane to the bottom, inducing a thin layer ( $\sim 5\text{-}20\mu\text{m}$ ) of the oxygen-rich dead zone to quench the photopolymerization. After repeating these processes, a 3D-architected polymer structure could be printed. **(B)** The relationships between the printing depth and the printing time for polymer inks with embedded chloroplasts of various weight concentrations. **(C)** Printed strips to illustrate the printing resolution ( $\sim 25\mu\text{m}$ ).

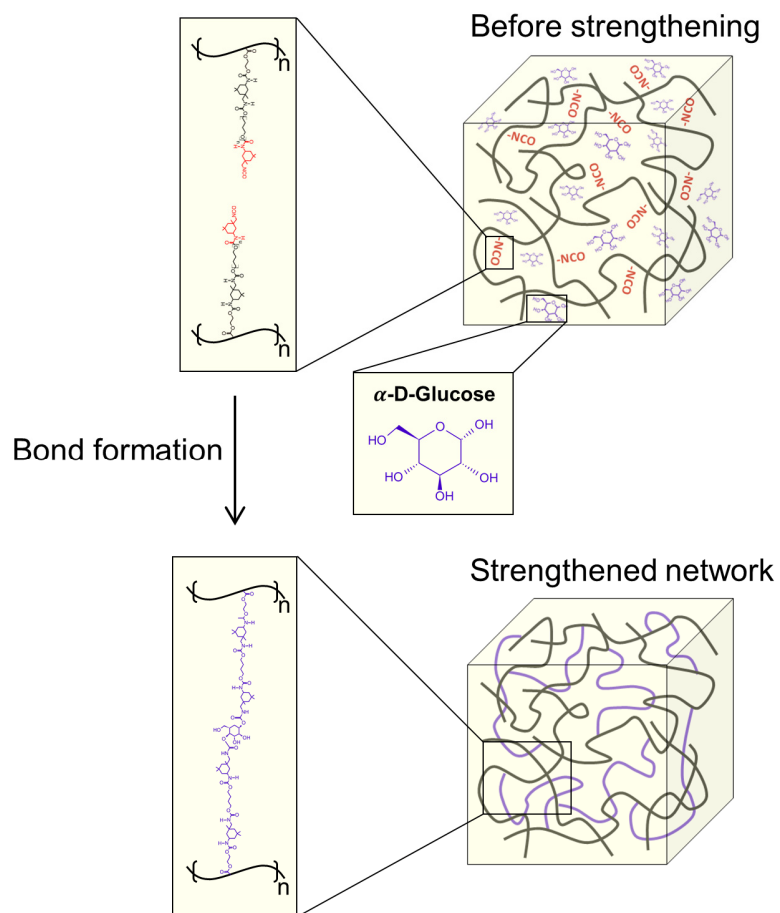


**Figure S4. Schematics to show the bond formation process between OH groups on the chloroplast-produced glucose with free NCO groups.** The zoom-in view of the initial network shows the chemical structure of free NCO groups and chloroplast-created glucose. The zoom-in view of the strengthened network shows the chemical structure with the new crosslink.

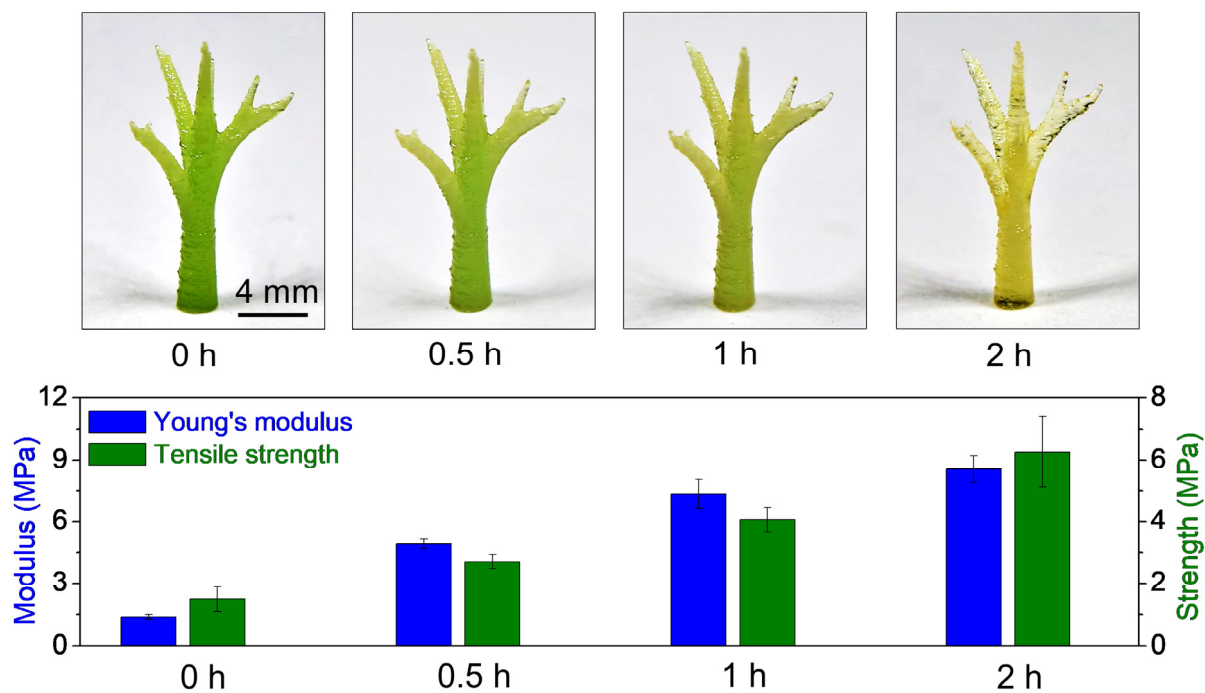


**Figure S5. Young's moduli and tensile strengths of the polymers in the 3D-printed tree-like structures with various light illumination periods.** The data of Young's modulus and tensile strengths were measured using dumbbell-shaped samples.

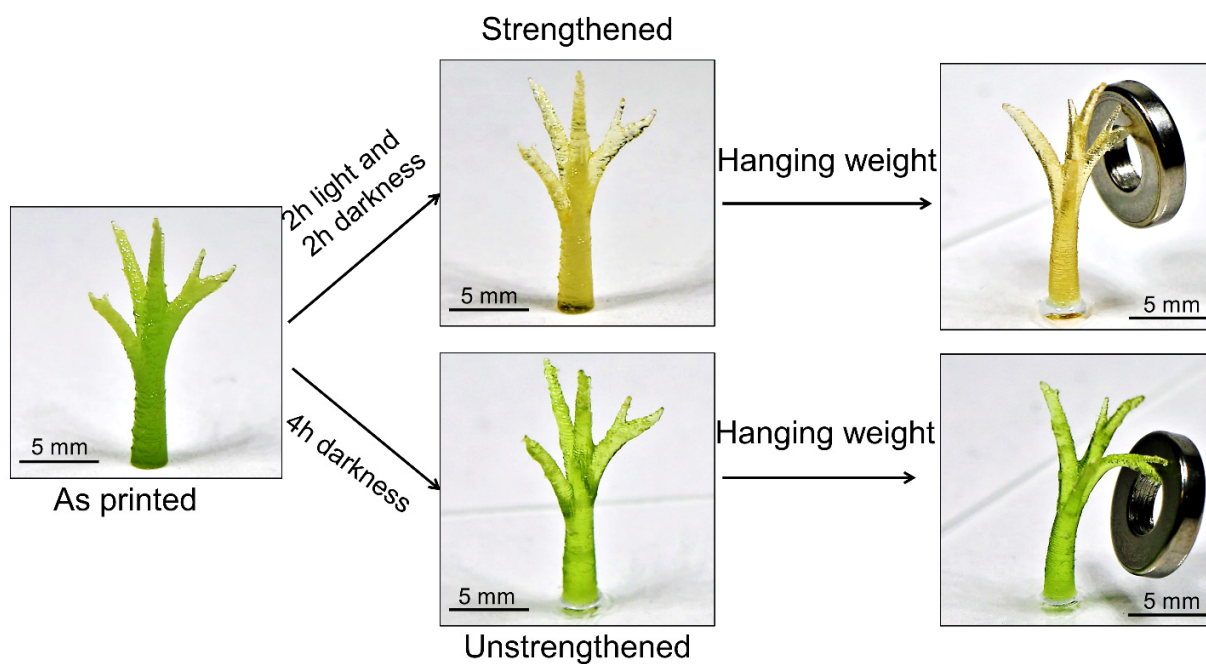


**Figure S6. Load sustaining ability 3D-printed tree-like structures.** In the top case, the tree structure went through 2-h light illumination (white light intensity  $69.3 \text{ W/m}^2$ ) and 2-h darkness. In the bottom case, the tree structure went through 4-h darkness. The mass of the metal ring is 1 g.

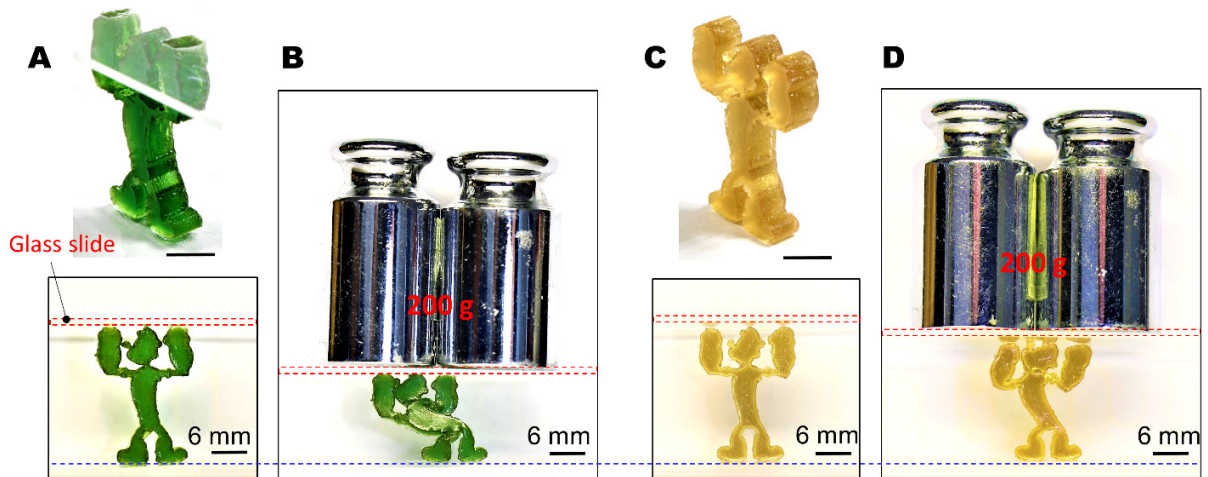


**Figure S7. Load-sustaining ability of the 3D-printed Popeye-like structures.** (A) Unstrengthened Popeye-like structure. (B) Unstrengthened Popeye-like structure loaded by a weight of 200 g. Its height reduces by 34.7%. (C) Strengthened Popeye-like structure. (D) Strengthened Popeye-like structure loaded by a weight of 200 g. Its height reduces by 7%.

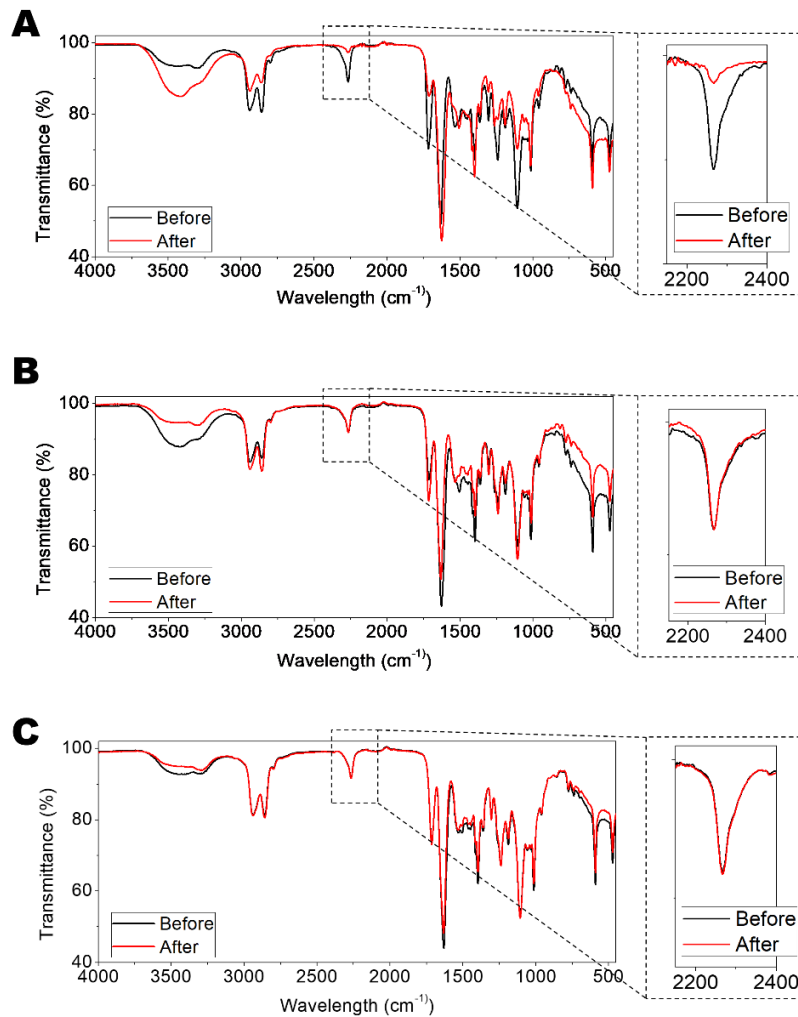


**Figure S8. Full FTIR spectra of samples with three groups.** (A) FTIR spectra of experimental group samples (with free NCO groups and embedded chloroplasts) before and after 4-h light illumination and 4-h darkness. (B) FTIR spectra of control 1 samples (with free NCO groups and embedded chloroplasts) before and after 8-h darkness. (C) FTIR spectra of control 2 samples (with free NCO groups but without embedded chloroplasts) before and after 4-h light illumination and 4-h darkness. The zoom-in view shows the spectra in the range of 2150 cm<sup>-1</sup> to 2400 cm<sup>-1</sup>, which indicates the concentration of the free NCO groups.

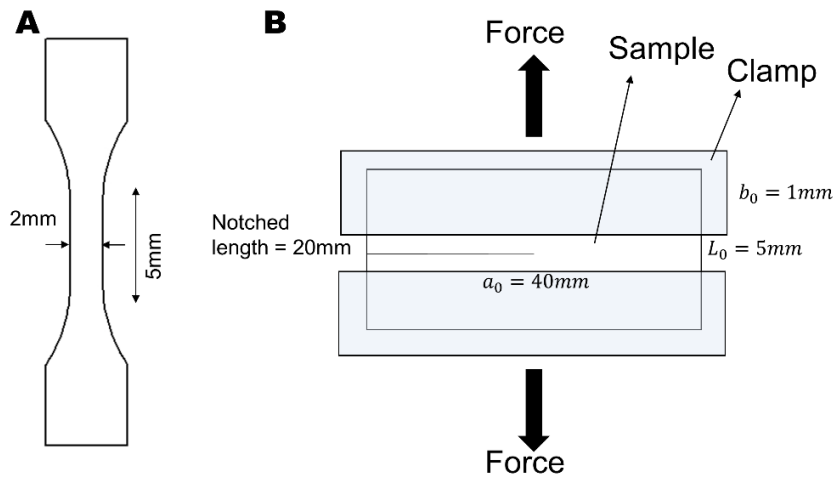


**Figure S9. Sample geometries of tensile and pure-shear fracture toughness tests.** (A) Geometry of a tensile test sample. The sample thickness is 2mm. (B) Geometry of a notched sample for pure-shear fracture toughness test. The fracture toughness test was conducted by testing an unnotched and notched sample. Each sample has a testing length  $a_0 = 40\text{ mm}$ , thickness  $b_0 = 1\text{ mm}$  and distance between two clamps  $L_0 = 5\text{ mm}$ . A 20-mm notch on the notched sample was prepared by using a razor blade. Both samples were tensile stretched with a strain rate of  $0.05\text{ s}^{-1}$  and recording using a high-speed camera to record the critical distance between the clamps when the crack starts propagating on the notched sample  $L_c$ . The fracture energy of the material was calculated as  $U(L_c)/(a_0 b_0)$ , where  $U(L_c)$  is the work done by the applied force before critical distance, illustrated as the area beneath the force-distance curve in the unnotched test.

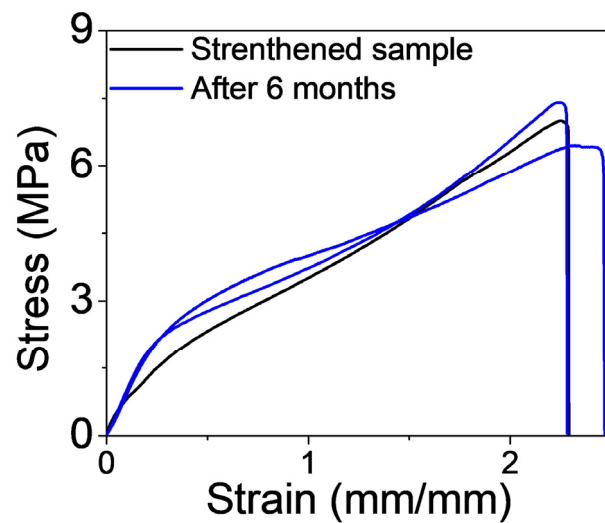


**Figure S10.** Stress-strain curves of a polymer sample right after the strengthening with 4-h light illumination and 4-h darkness and the strengthened polymers after 6 months. The employed polymer sample was 3D-printed with polymer inks with free NCO groups and embedded chloroplasts. The results show that the strengthened polymer maintains its Young's modulus and tensile strength after 6 months.



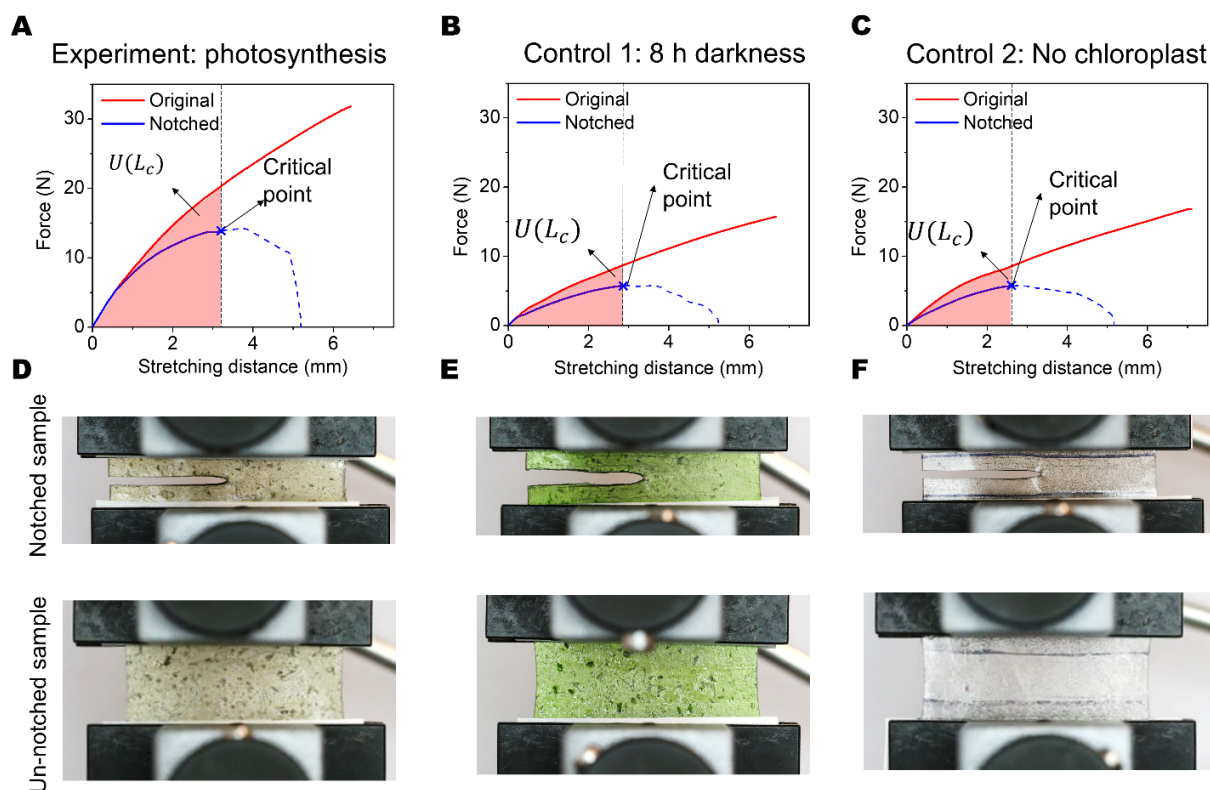


**Figure S11. Force-distance curves and experiment images for fracture-toughness tests.** Force-distance curves of notched and unnotched samples under uniaxial stretch for (A) the experimental case, (B) control 1 case, and (C) control 2 case. The experimental sample has free NCO groups and embedded chloroplasts, and undergoes 4-h light illumination and 4-h darkness. The control 1 sample has free NCO groups and embedded chloroplasts, and undergoes 8-h darkness. The control 2 sample has free NCO groups but no embedded chloroplasts, and undergoes 4-h light illumination and 4-h darkness. The critical points indicate the point when the crack starts propagating on the notched sample. Sample images of notched and unnotched samples under uniaxial stretch for (D) the experimental case, (E) control 1 case, and (F) control 2 case.

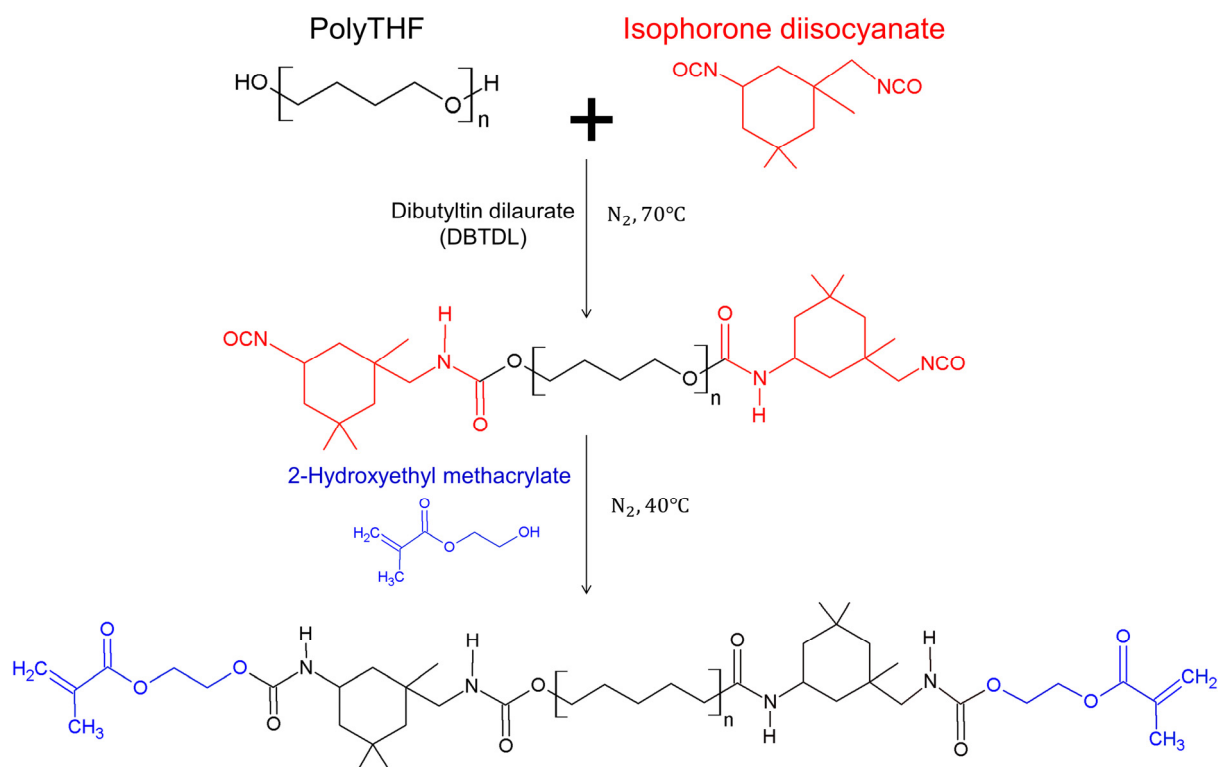


**Figure S12. Synthesis of polymer resin with only acrylate groups but without free NCO groups.** 0.01 mole of PolyTHF was preheated at 100°C and exposed to a nitrogen environment for 1 h to remove moisture and oxygen. 0.02 mole of IPDI, 10 wt% of DMAc and 1 wt% of DBTDL were mixed with preheated PolyTHF at 70°C and stirred with a magnetic stir bar for 1 h. After reducing the temperature to 40°C, 0.02 mole of HEMA was added and mixed for 1 h to complete the synthesis.

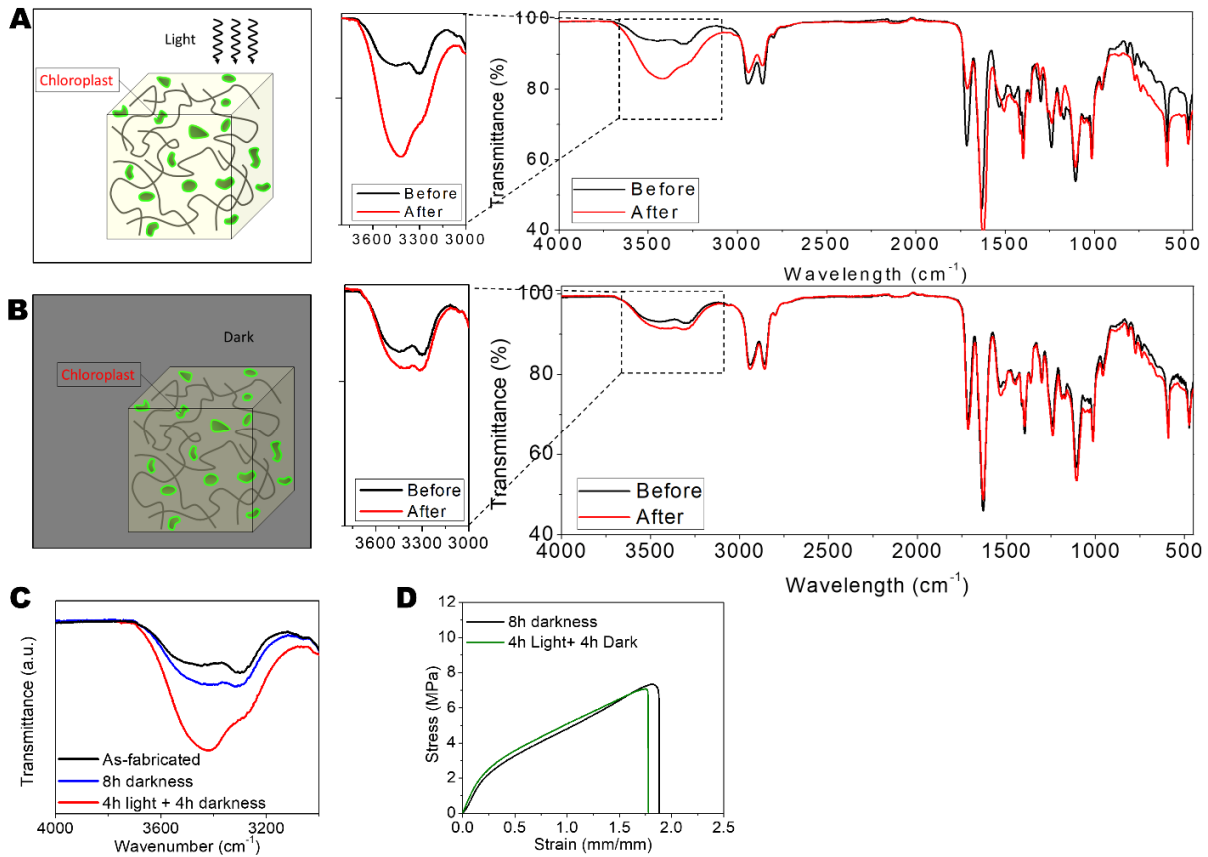


**Figure S13. Experiments on polymer samples with embedded chloroplasts but without free NCO groups.** (A) The polymer samples with embedded chloroplasts but without free NCO groups went through 4-h light illumination (white light intensity  $69.3 \text{ W/m}^2$ ) and 4-h darkness. (B) The polymer samples with embedded chloroplasts but without free NCO groups went through 8-h darkness. (C) The zoom-in views showing the spectra in the range of  $3000 \text{ cm}^{-1}$  to  $3800 \text{ cm}^{-1}$ , which indicates the concentration of OH groups<sup>18</sup>. (D) Tensile stress-strain curves of polymer samples with embedded chloroplasts but without free NCO groups after 4-h light illumination and 4-h darkness, and 8-h darkness.

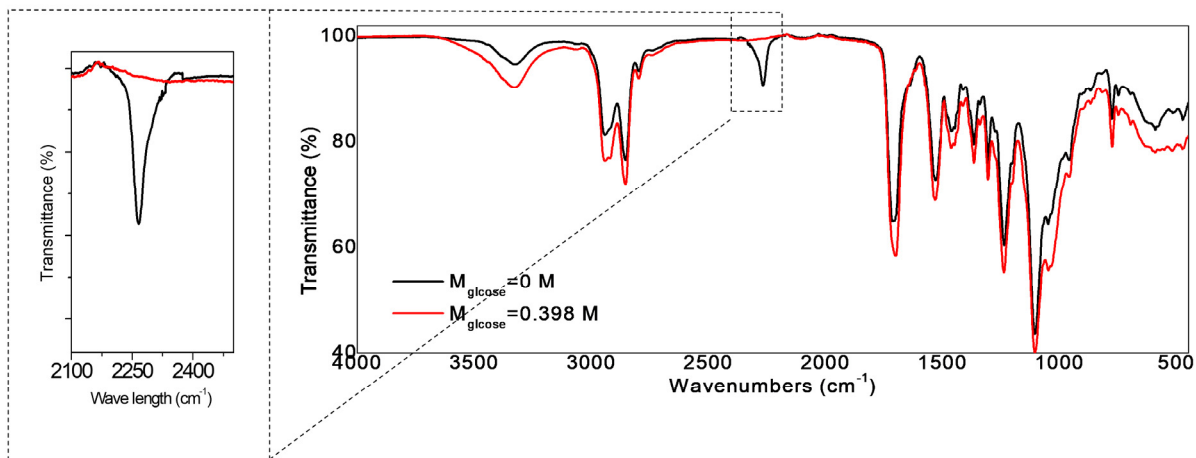


**Figure S14.** Full FTIR spectra of polymer ink with free NCO groups but without embedded chloroplasts before and after being mixed with 0.398 mol/L of glucose. The zoom-in view shows the spectrum in the range of 2100 cm<sup>-1</sup> to 2500 cm<sup>-1</sup>, which indicates the concentration of free NCO groups.

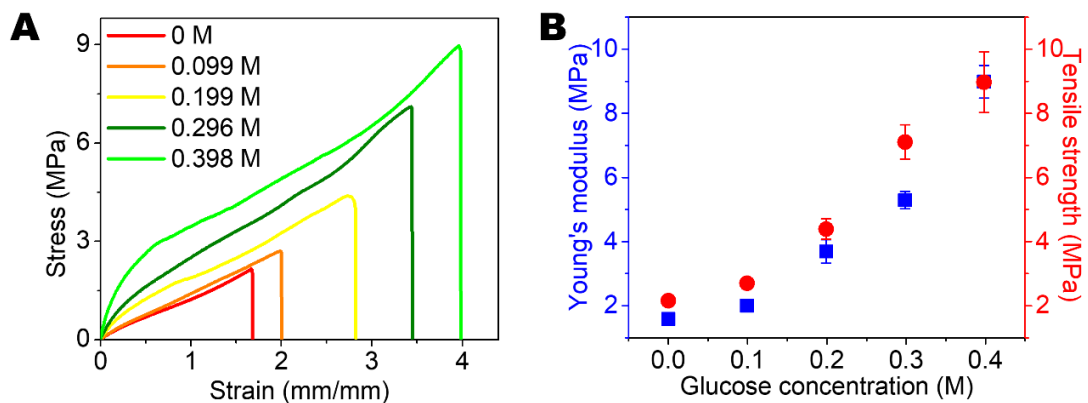


**Figure S15.** (A) Uniaxial tensile stress-strain curves of polymer samples with free NCO groups and various concentrations of glucose. (B) Young's moduli and tensile strengths in functions of the glucose concentration. The error bars represent the standard deviations of 3-5 samples.

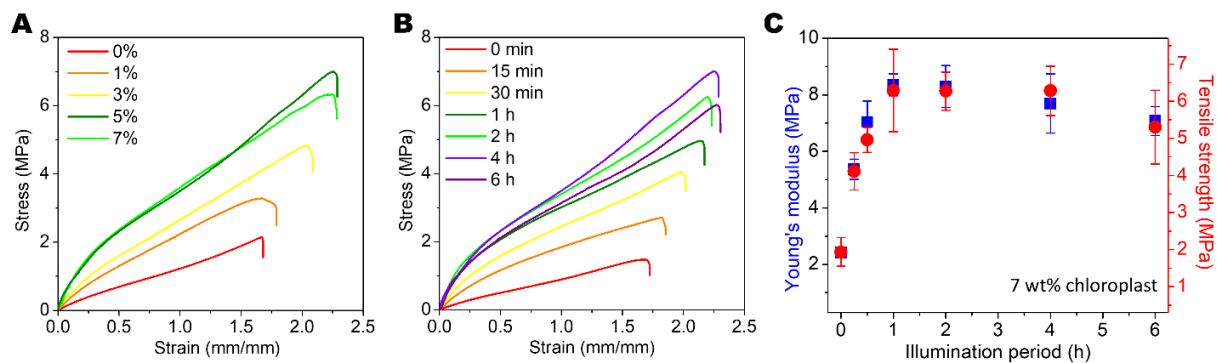


**Figure S16.** (A) Uniaxial tensile stress-strain curves of polymer samples with free NCO groups and embedded chloroplasts of various weight concentrations. (B) Uniaxial tensile stress-strain curves of polymer samples with free NCO groups and 5 wt% chloroplasts after the photosynthesis processes with various light illumination periods. (C) Young's moduli and tensile strengths of experimental samples with 7 wt% chloroplasts after the photosynthesis processes with various light illumination periods.

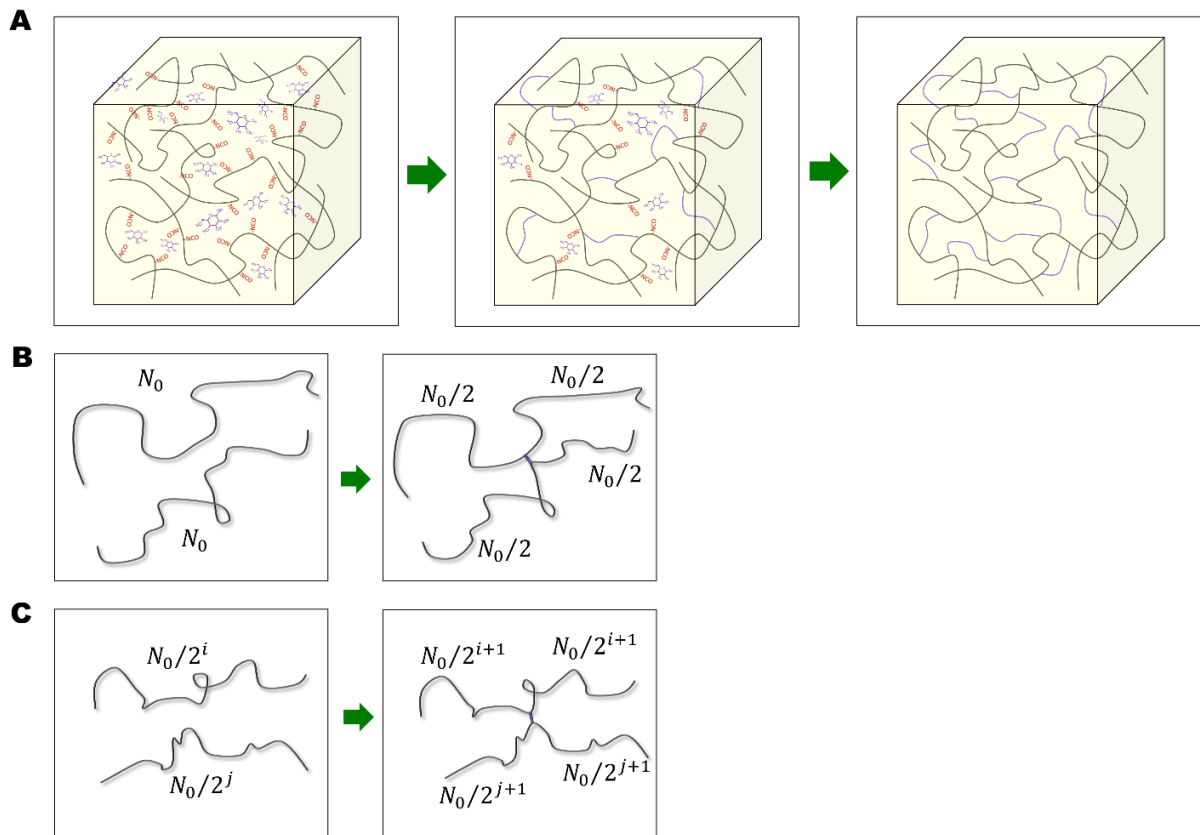


**Figure S17. Schematics for the polymer network.** (A) Schematics to show the formation of additional crosslinks through the reaction between the free NCO groups and the glucose. (B) Schematics to show the formation of one crosslink between two chains with the length of  $N_0$ . We assume each chain with the initial length of  $N_0$  becomes two chains with the length of  $N_0/2$ . (C) Schematics to show the formation of one crosslink between a chain with the length of  $N_0/2^i$  and a chain with the length of  $N_0/2^j$ . We assume the crosslink formed between a chain with the length of  $N_0/2^i$  and a chain with the length of  $N_0/2^j$  induces four chains with respective half lengths, where  $i = 0,1,2 \dots$  and  $j = 0,1,2 \dots$ .

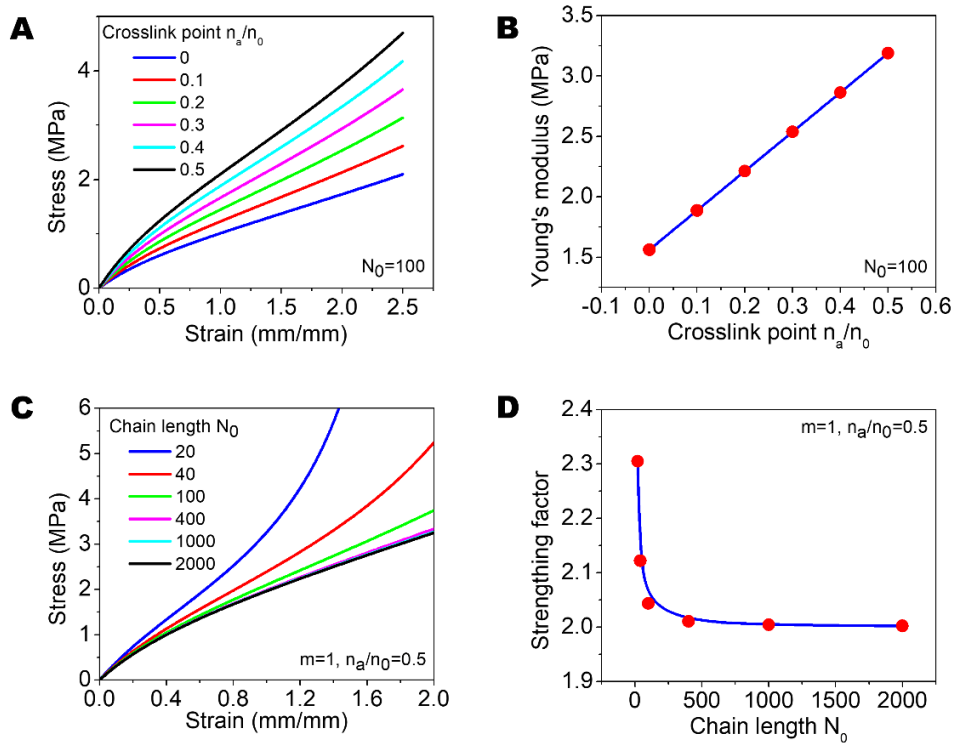


**Figure S18. Theoretical results for step number  $m=1$ .** (A) Nominal tensile stress-strain curves for various normalized additional crosslink density  $n_a/n_0$ . (B) The Young's modulus of the polymer in a function of the normalized additional crosslink density  $n_a/n_0$ . The Young's modulus is calculated from the stress-strain curve within 10% strain. (C) Nominal tensile stress-strain curves for various initial chain length  $N_0$  and  $n_a/n_0 = 0.5$ . (D) Strengthening factor in a function of the chain length for  $m = 1$  and  $n_a/n_0 = 0.5$ . The strengthening factor is defined as the strengthened Young's modulus normalized by the unstrengthened Young's modulus.



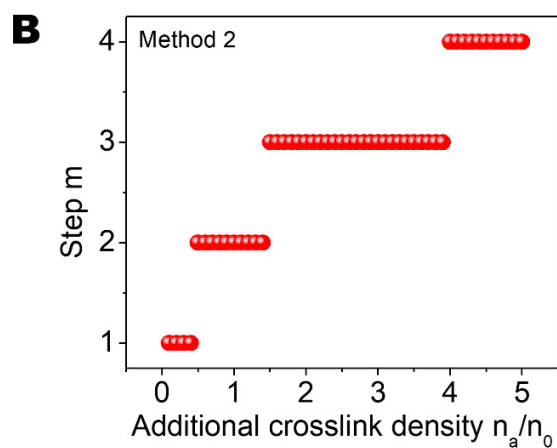
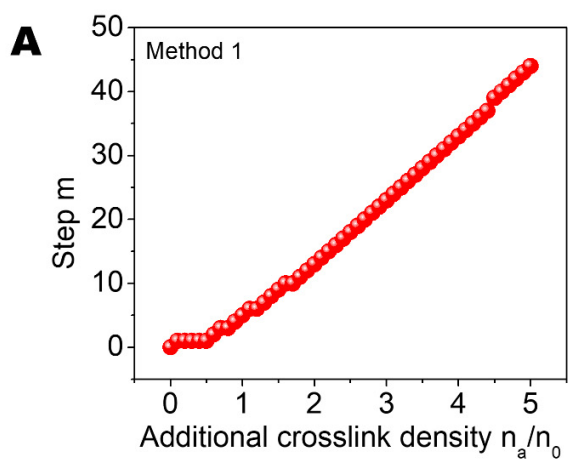


**Figure S19.** Relationships between the step number  $m$  and additional crosslink density  $n_a/n_0$  for (A) method 1 and (B) method 2.

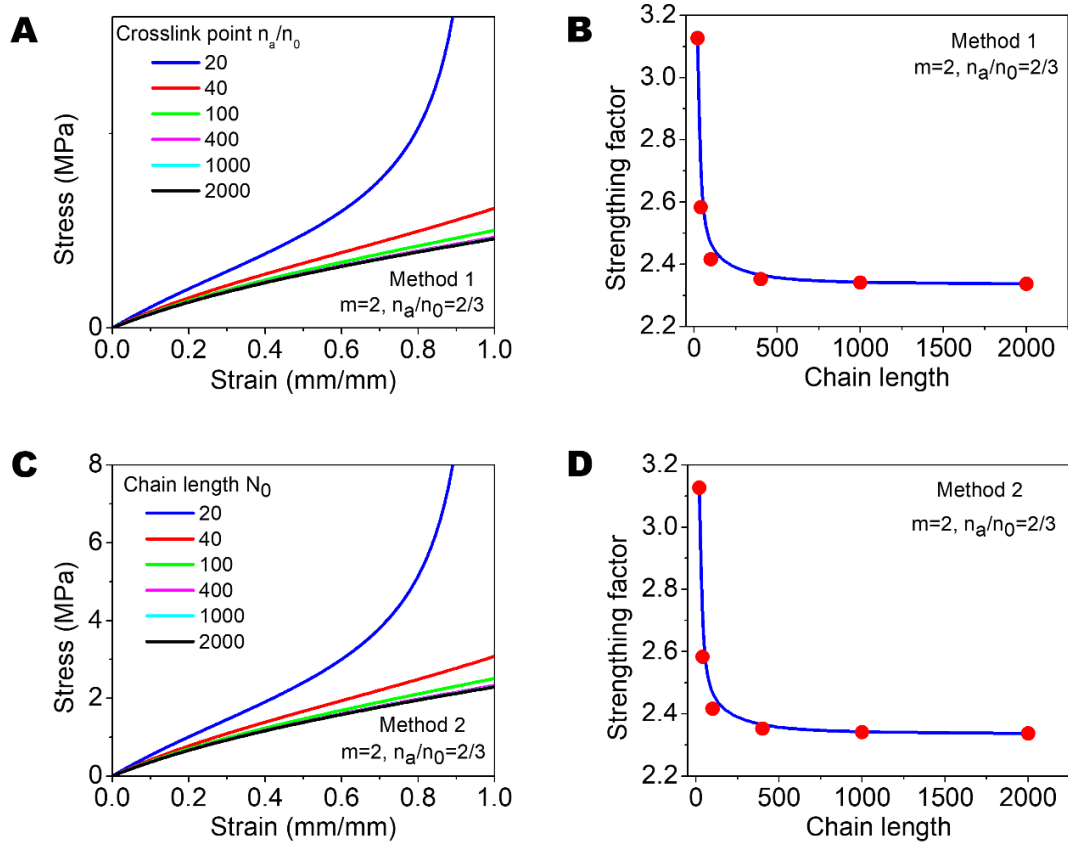


**Figure S20. Theoretical results for  $m = 2$  and  $n_a/n_0 = 2/3$ .** Stress-strain curves and strengthening factors for various initial chain lengths  $N_0$  based on (AB) method 1 and (CD) method 2.

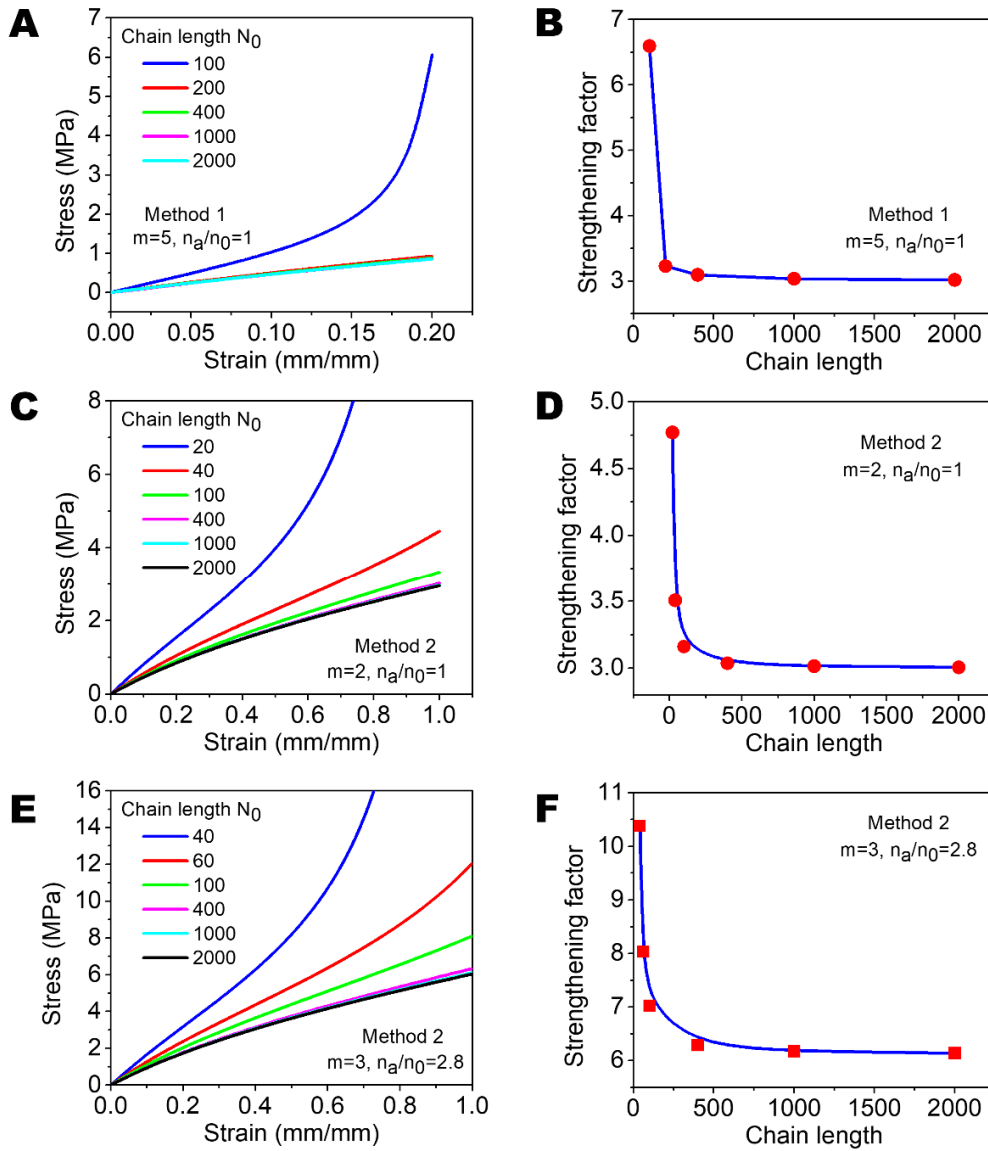


**Figure S21. Theoretical results for  $n_a/n_0 > 2/3$ .** Stress-strain curves and strengthening factors for various initial chain lengths  $N_0$  and (AB)  $m = 5$  and  $n_a/n_0 = 1$  (method 1), (CD)  $m = 2$  and  $n_a/n_0 = 1$  (method 2), and (EF)  $m = 3$  and  $n_a/n_0 = 3.05$  (method 2).

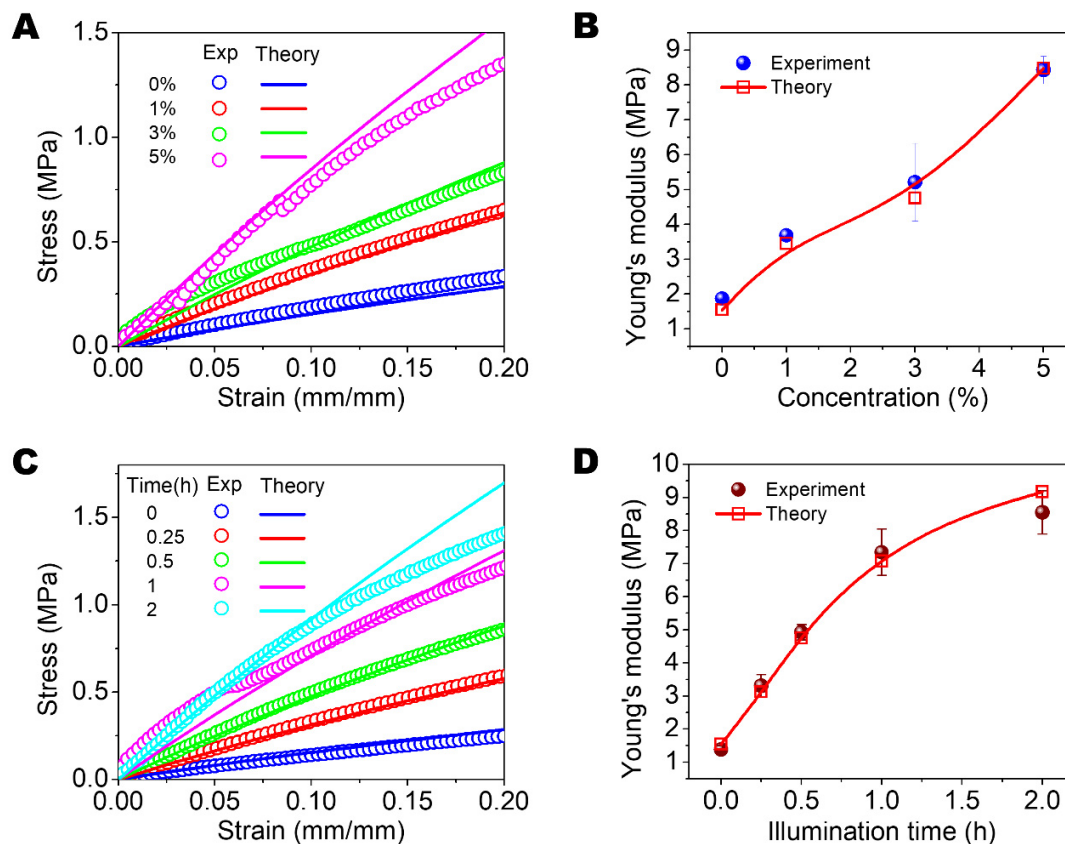


**Figure S22. Comparison between the theory and experiment.** (A) Stress-strain curves and (B) Young's moduli of polymer samples with free NCO groups and chloroplasts of various weight concentrations after 4-h light illumination and 4-h darkness. (C) Stress-strain curves and (D) Young's moduli of polymer samples with free NCO groups and 5 wt% chloroplasts after various illumination periods and the corresponding periods of darkness. The parameters used to calculate the theoretical results are listed in **Table S2**. The error bars in (B) and (D) represent standard deviations of 3-5 samples.

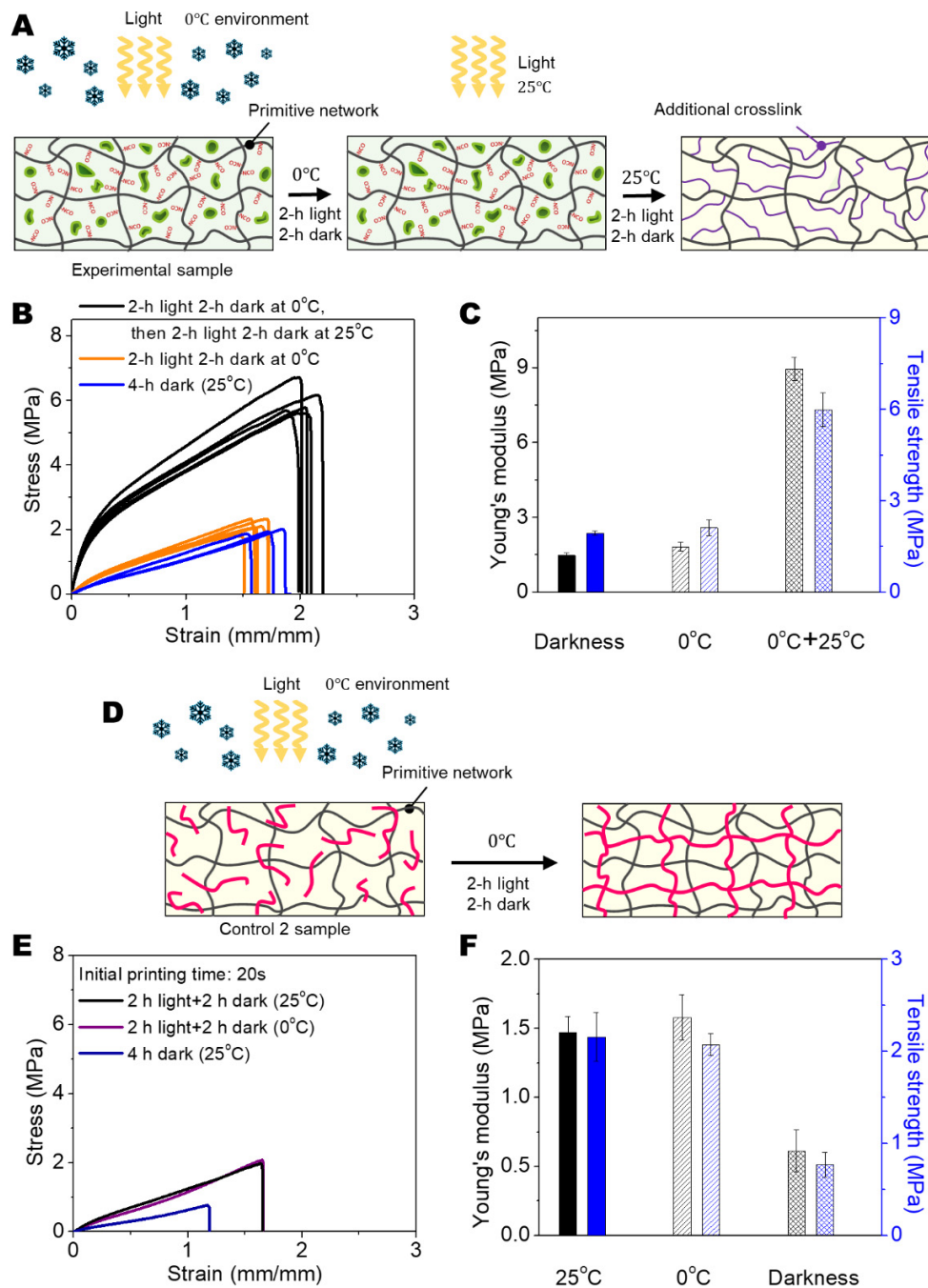


**Figure S23.** Effect of chilling temperature on the proposed hybrid synthetic-living material and traditional photopolymer. (A) Schematics to illustrate the procedure for an experimental sample first undergoing 2-h light illumination and 2-h darkness at 0°C, and then undergoing 2-h light illumination and 2-h darkness at 25°C. (BC) Stress-strain curves, Young's moduli, and tensile strengths of the processed experimental samples at three states: after 4-h darkness, after 2-h light and 2-h darkness at 0°C, and after 2-h light and 2-h darkness at 0°C followed by 2-h light and 2-h darkness at 25°C. The error bars represent standard deviations of 3-5 samples. Results show that chilling temperature can temporarily freeze the living activity of the embedded chloroplasts. (D)

Schematics to illustrate the post-curing procedure for a partially-crosslinked control 2 sample undergoing 2-h light illumination and 2-h darkness at 0°C. Since the control 2 sample can be fully crosslinked with light illumination of 60s, we employed 20s to enable a partial crosslinking. (EF) Stress-strain curves, Young's moduli, and tensile strengths of the processed control 2 samples at three states: after 2-h light and 2-h darkness at 25°C, after 2-h light and 2-h darkness at 0°C, and after 4-h darkness at 25°C. The error bars represent standard deviations of 3-5 samples. Results show that the post-curing of a partially-crosslinked photoresin cannot be frozen by a chilling temperature.

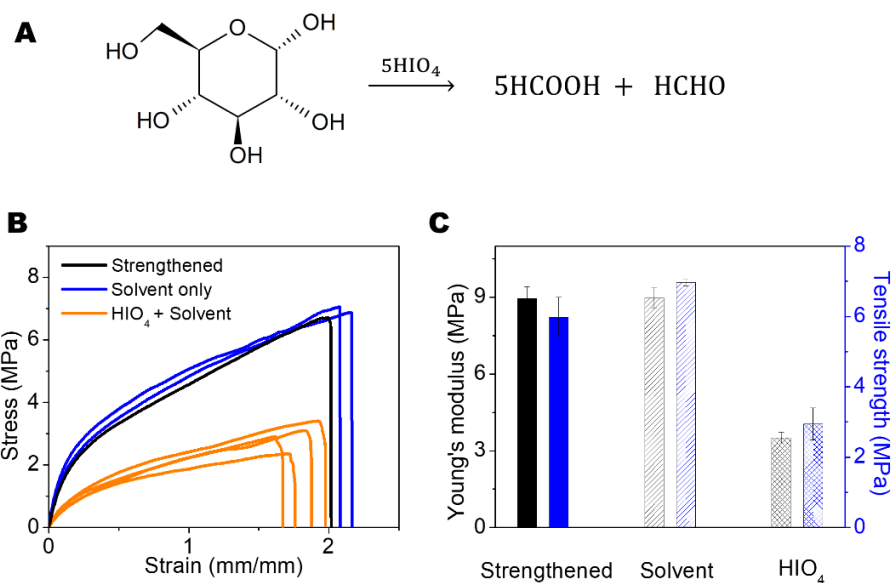


**Figure S24. Cleavage of glucose crosslinkers with period acids (HIO<sub>4</sub>).** (A) Chemical reaction for cleaving a glucose molecule with period acids. (BC) Stress-strain curves, Young's moduli, and tensile strengths of strengthened samples, and strengthened samples treated with solvent DMAc only, and strengthened samples treated with HIO<sub>4</sub> solution (2 M HIO<sub>4</sub> with solvent DMAc). The mechanical tests were carried out after evaporating the residual solvents. Results show that the HIO<sub>4</sub> can cleave the glucose crosslinkers to reverse the strengthened samples back to the soft state. The error bars represent standard deviations of 3-5 samples.

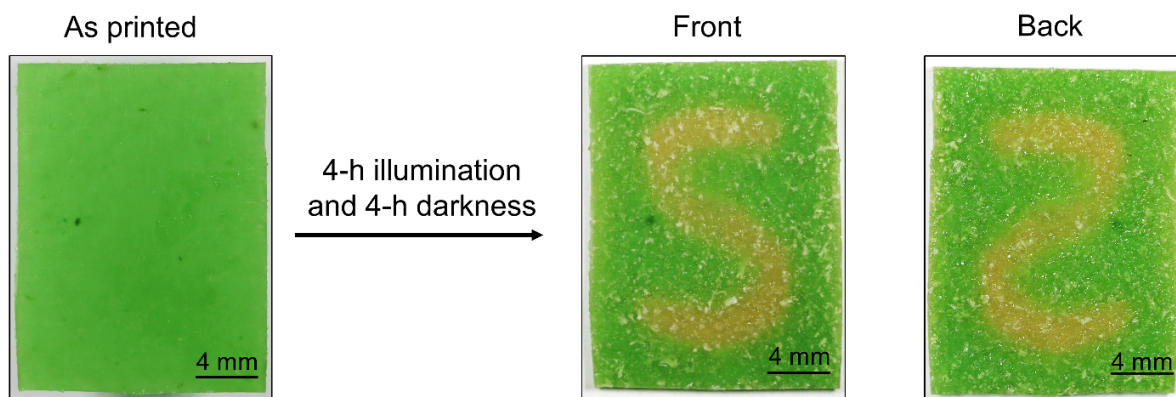


**Figure S25.** Sample images of a locally strengthened sample through a patterned light with an “S” shape.



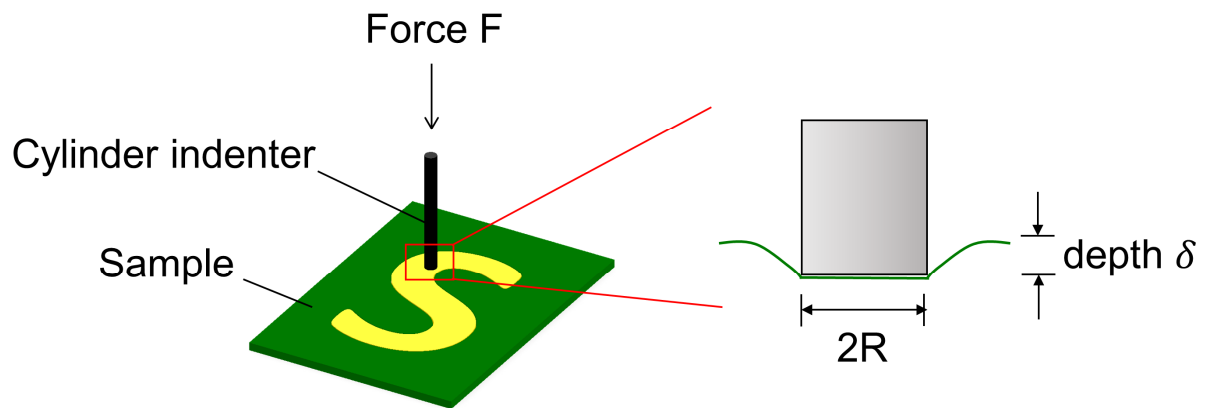


**Figure S26. Experimental set-up of an indentation test.** A round-flat end cylinder indenter with radius  $R=1$  mm is loaded on the Instron mechanical tester to indent the sample by applying force  $F$  to a certain indentation depth  $\delta$ . The Young's modulus is calculated as  $E = F(1 - \nu^2)/(2R\delta)$ , where  $\nu$  is the Poisson's ratio.

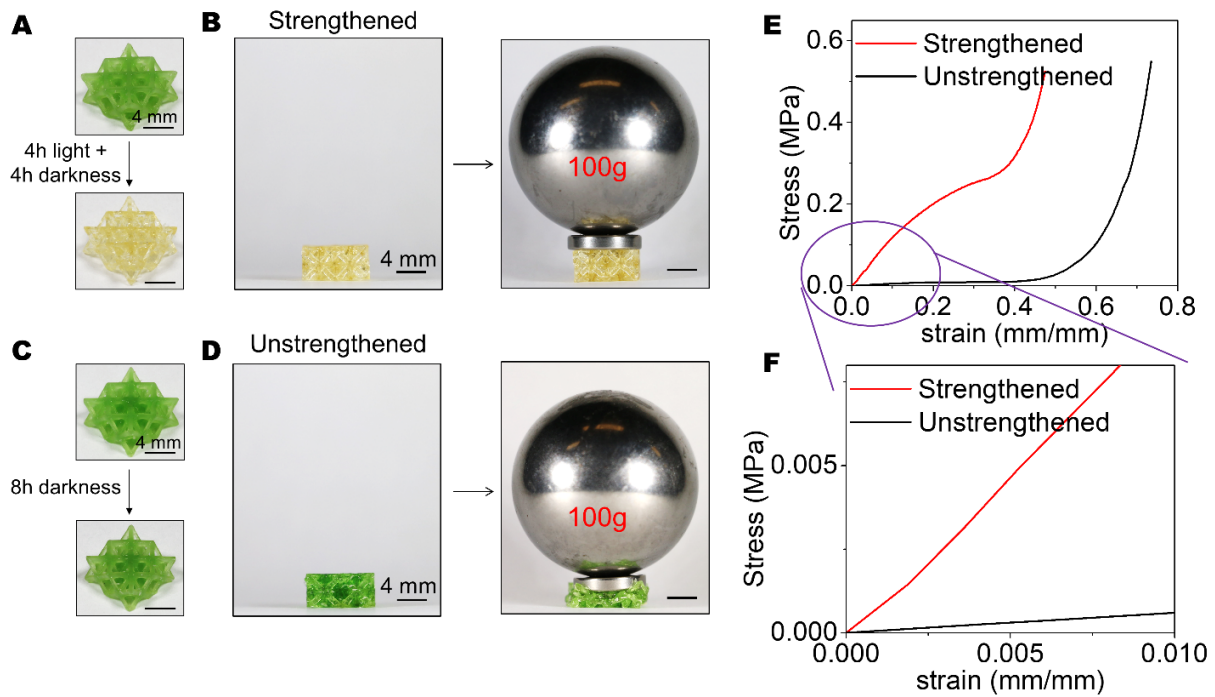


**Figure S27. Strengthening of Octet lattice with homogeneous light illumination.** (AB) 3D-printed Octet lattice structure with free NCO groups and embedded chloroplasts went through 4-h light illumination and 4-h darkness and sustained a 100g weight (lattice weight 0.12 g). (CD) 3D-printed Octet lattice structure with free NCO groups and embedded chloroplasts went through 8-h darkness and sustained a 100g weight. (E) Compressive stress-strain curves of the strengthened and unstrengthened Octet lattice structures. (F) Zoom-in view of the compressive stress-strain curve of the 3D-printed Octet lattice structure. The strengthened lattice exhibits Young's modulus that is 20 times that of the non-strengthened lattice. The scale bars represent 4 mm.

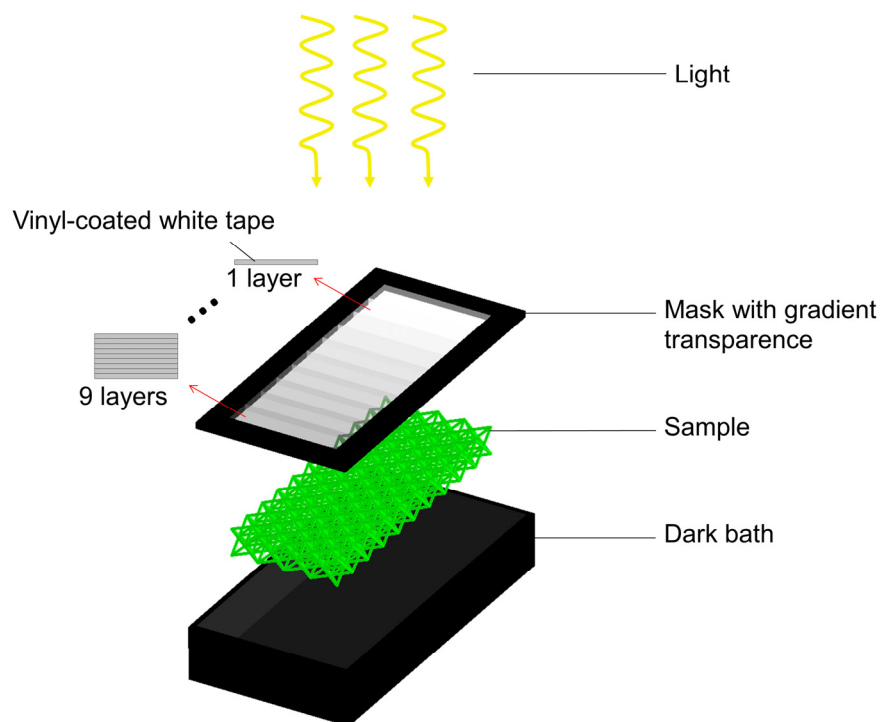


**Figure S28. Schematic to show the experimental setup for the 3D-printed structures with a gradient light intensity.** A transparent cover was attached with different layers of vinyl-coated white tape and covered on top of the printed sample. The entire setup was then placed in the chamber with light intensity varies from 0 to  $69.3 \text{ W/m}^2$  on the long edge direction of the sample for each unit distance (2 mm).

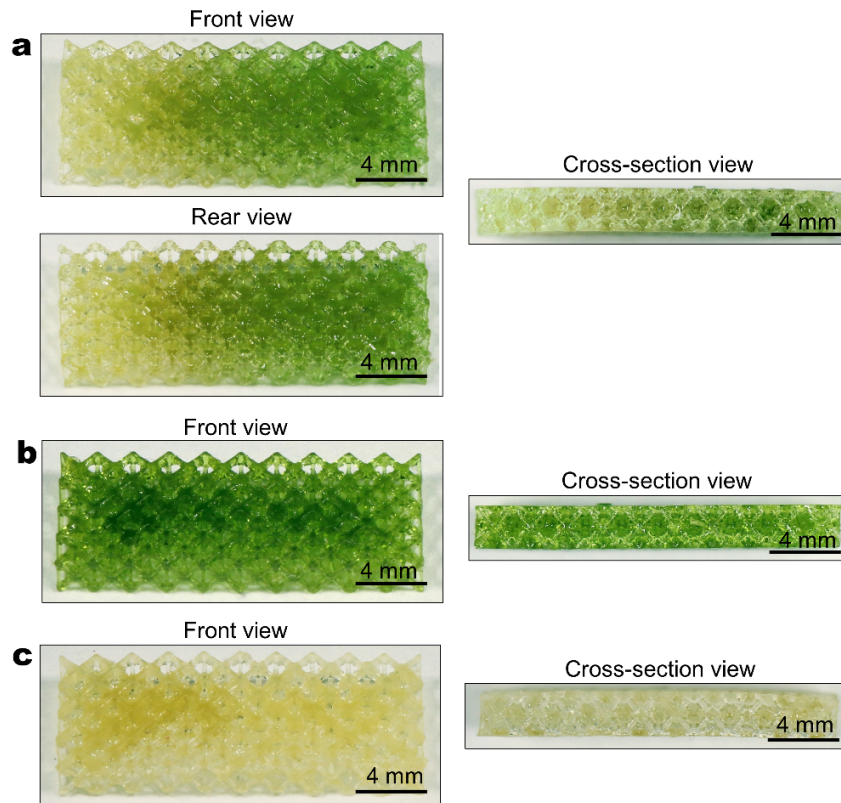


**Figure S29.** (a) Front, rear, and cross-section views of the functionally-graded lattice structure. (b) Front and cross-section views of the (b) fully-soft and (c) fully-stiffened lattice structures.

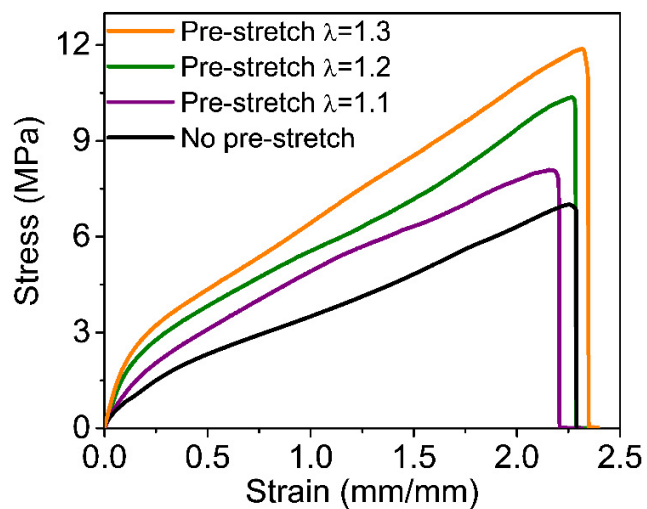


**Figure S30.** Stress-strain curves of experimental polymer samples (with free NCO groups and embedded chloroplasts) with various pre-stretches after the photosynthesis process (4-h light and 4-h darkness).

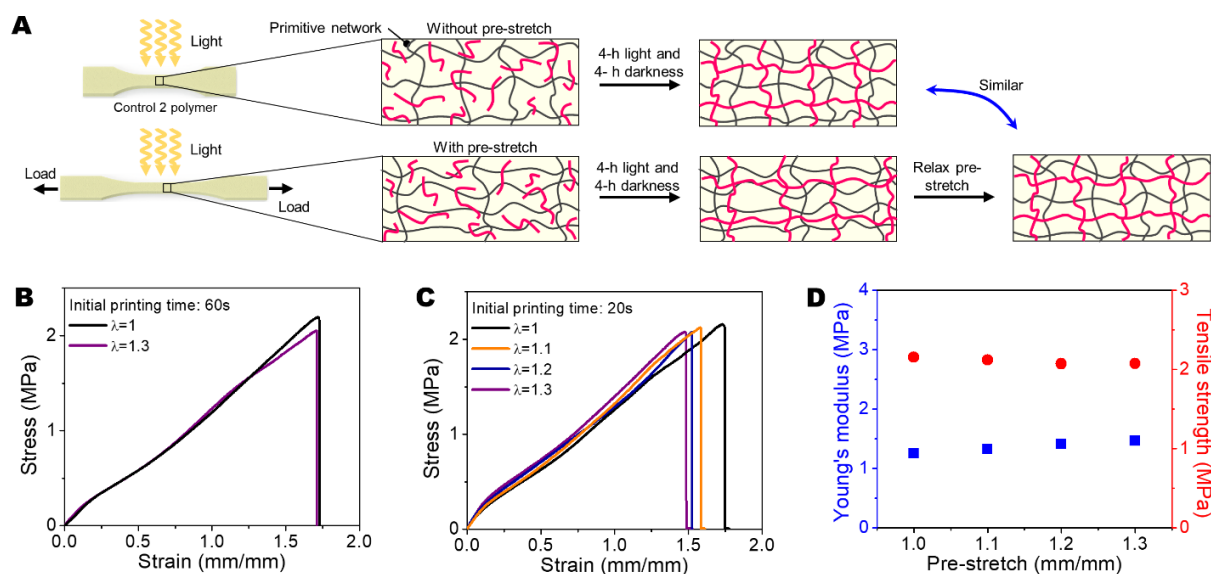


**Figure S31.** Effect of pre-stretch on the mechanical property of post-cured control 2 polymer (with free NCO groups but without chloroplasts). (A) Schematics to illustrate the post-curing of control 2 samples without and with a pre-stretch. The post-curing condition is the same as the photosynthesis condition: 4-h light illumination and 4-h darkness. (B) Stress-strain curves of post-cured control 2 samples (printed with 60 s, close to fully cured) without a pre-stretch and with a pre-stretch of 1.3. (C) Stress-strain curves of post-cured control 2 samples (printed with 20 s, partially-cured) without a pre-stretch ( $\lambda = 1$ ) and with various pre-stretches ( $\lambda = 1.1 - 1.3$ ). (D) The Young's moduli and tensile strengths of the post-cured control 2 samples (printed with 20 s, partially-cured) in functions of the pre-stretch  $\lambda$ .

Experimental procedure: The samples were prepared by 3D printing process using control 2 polymer ink (with free NCO groups but without chloroplasts) under different light exposure time (20 s or 60 s). When the light exposure time was 60 s, the sample was fully crosslinked; when the light exposure time was 20 s, the sample was partially-cured. The fabricated samples were then uniaxially pre-stretched with various stretches ( $\lambda = 1 - 1.3$ ) and undergone 4-h light illumination and 4-h darkness. The pre-stretched section of the samples was then cut into dumbbell-like shape, and uniaxially stretched until rupture with a strain rate of  $0.05 \text{ s}^{-1}$ .

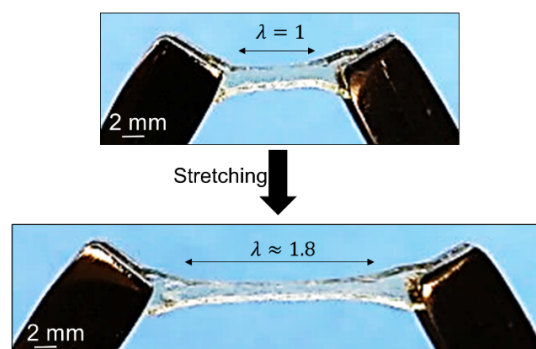


**Figure S32.** Stretching of a healed sample after 4-h light illumination and 4-h darkness.

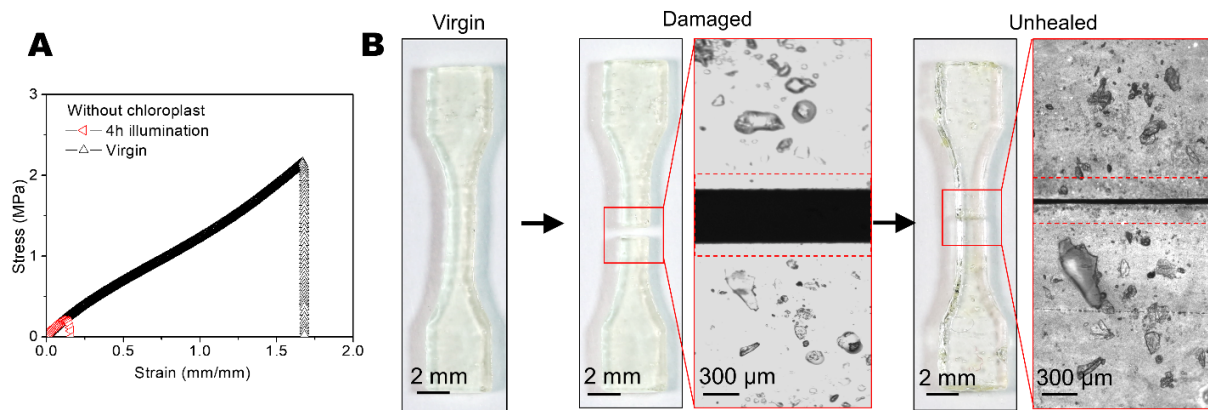


**Figure S33. Self-healing of the control sample.** (A) Uniaxial tensile stress-strain curves of control samples with free NCO groups but without embedded chloroplasts at the virgin state and after the healing process (4-h illumination and 4-h darkness). (B) control samples and interfacial microscope images at the virgin, damaged, and healed states.



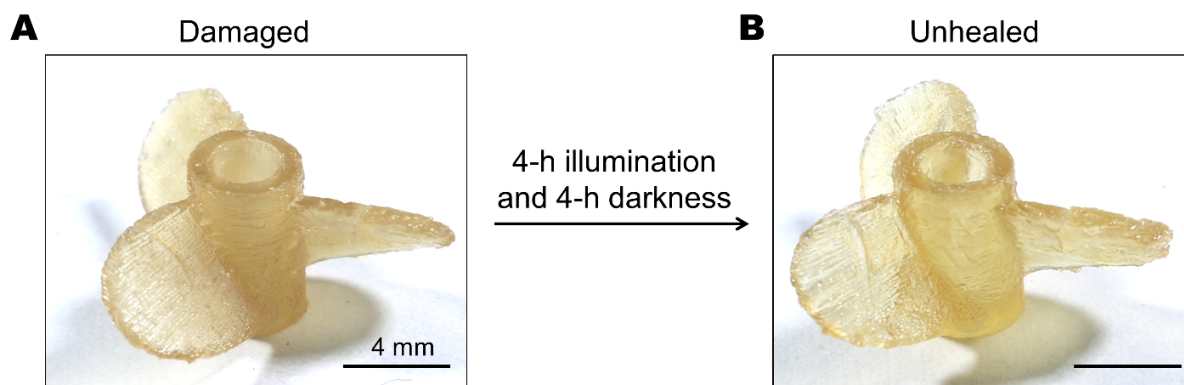


**Figure S34. Healing process of 3D-printed propeller made by control 2 polymer with free NCO group but without embedded chloroplasts.** (A) Image of sample damaged with sharp blade (B) Image of the unhealed sample after 4-h light illumination and 4-h darkness. The scale bars represent 4 mm.

**Table S1.**

Experimental data for measuring the mass percentage of water within the extracted chloroplast.

Sample #	The initial mass of extracted chloroplast (g)	Mass after 8-h evaporation in a dark environment (g)	Mass of water (g)	Mass percentage of water (%)
1	0.3092	0.0592	0.25	80.9
2	0.3019	0.0529	0.249	82.5
3	0.3097	0.0567	0.253	81.7
4	0.3042	0.0452	0.259	85.1
5	0.3	0.041	0.259	86.3
6	0.3075	0.0405	0.267	86.8
			Mean	83.9
			Standard deviation	2.5

**Table S2.**

Parameters used for the theoretical calculations.

<b>Parameter</b>	<b>Physical meaning</b>	<b>Figs. S22AB</b>	<b>Figs. S22CD</b>
$N_0$	Initial chain length	400	400
$n_0$	Initial chain number density ( $\text{m}^{-3}$ )	$4.5 \times 10^{19}$	$4.5 \times 10^{19}$
$T$	Temperature (K)	300	300
$n_a/n_0$	Normalized additional crosslink density	0 for 0% 0.6 for 1% 1.1 for 3% 2.1 for 5%	0 for 0 h 0.5 for 0.25 h 1 for 0.5 h 1.8 for 1 h 2.3 for 2h

**Movie S1.**

A movie to illustrate the photosynthesis-assisted healing of a dumbbell-shaped sample. The sample was 3D-printed with a polymer ink with free NCO groups and 5 wt% embedded chloroplasts. Then, the sample was cut into two parts with a blade, followed by being brought into contact under 4-h light illumination and 4-h darkness. Then the healed sample was stretched by two twisters.

**Movie S2.**

A movie to illustrate the comparison of 3D-printed experimental and control propellers in healing fractures in their structures. In the first part, a 3D-print propeller with the experimental polymer ink with free NCO groups and 5 wt% embedded chloroplasts was damaged by making cracks in its sectors. The sector cracks were healed by a photosynthesis process with 4-h illumination and 4-h darkness. The healed propeller that was assembled on a remotely controlled boat could facilitate the forward movement of the boat. In the second part, a 3D-print propeller with the control polymer ink with free NCO groups but without embedded chloroplasts was damaged by making cracks on its sectors. The sector cracks could not be healed by a photosynthesis process with 4-h illumination and 4-h darkness. The unhealed propeller that was assembled on a remotely controlled boat could not facilitate the forward movement of the boat.

## References

- 1 Treloar, L. R. G. *The physics of rubber elasticity*. (Oxford University Press, USA, 1975).
- 2 Arruda, E. M. & Boyce, M. C. A three-dimensional constitutive model for the large stretch behavior of rubber elastic materials. (1993).
- 3 Rubinstein, M. & Colby, R. H. *Polymer physics*. Vol. 23 (Oxford university press New York, 2003).
- 4 Yu, K., Xin, A., Feng, Z., Lee, K. H. & Wang, Q. Mechanics of self-healing thermoplastic elastomers. *Journal of the Mechanics and Physics of Solids* **137**, 103831 (2020).
- 5 Xin, A., Zhang, R., Yu, K. & Wang, Q. Mechanics of electrophoresis-induced reversible hydrogel adhesion. *Journal of the Mechanics and Physics of Solids* **125**, 1-21 (2019).
- 6 Yu, K., Xin, A. & Wang, Q. Mechanics of light-activated self-healing polymer networks. *Journal of the Mechanics and Physics of Solids* **124**, 643-662 (2019).
- 7 Yu, K., Xin, A. & Wang, Q. Mechanics of self-healing polymer networks crosslinked by dynamic bonds. *Journal of the Mechanics and Physics of Solids* **121**, 409-431 (2018).
- 8 Wang, Q., Gao, Z. & Yu, K. Interfacial self-healing of nanocomposite hydrogels: Theory and experiment. *Journal of the Mechanics and Physics of Solids* **109**, 288-306 (2017).
- 9 Wang, Q. & Gao, Z. A constitutive model of nanocomposite hydrogels with nanoparticle crosslinkers. *Journal of the Mechanics and Physics of Solids* **94**, 127-147 (2016).
- 10 Wang, Q., Gossweiler, G. R., Craig, S. L. & Zhao, X. Mechanics of mechanochemically responsive elastomers. *Journal of the Mechanics and Physics of Solids* **82**, 320-344 (2015).
- 11 Joly, D. & Carpentier, R. in *Photosynthesis Research Protocols* Vol. 684 (ed Robert Carpentier) 321-325 (Humana Press, 2011).
- 12 Von Caemmerer, S. *Biochemical models of leaf photosynthesis*. (Csiro publishing, 2000).
- 13 Lawlor, D. W. *Photosynthesis: molecular, physiological and environmental processes*. (Longman scientific & technical, 1993).
- 14 Gregory, R. P. F. *Biochemistry of photosynthesis*. Vol. 5 (Wiley London, 1977).
- 15 Matsunaga, K., Sato, K., Tajima, M. & Yoshida, Y. Gas permeability of thermoplastic polyurethane elastomers. *Polymer journal* **37**, 413-417 (2005).
- 16 Xiao, H., Ping, Z. H., Xie, J. W. & Yu, T. Y. Permeation of CO<sub>2</sub> through polyurethane. *Journal of Applied Polymer Science* **40**, 1131-1139 (1990).
- 17 <https://www.co2.earth/daily-co2>.
- 18 Korolevich, M. V., Zhbakov, R. G. & Sivchik, V. V. Calculation of absorption-band frequencies and intensities in the ir-spectrum of alpha-d-glucose in a cluster. *Journal of Molecular Structure* **220**, 301-313 (1990).